New Avenues : Weak Lensing And Model Independent Primordial Power Spectrum Reconstruction

Rajorshi Sushovan Chandra
IUCAA

May 24, 2021

Overview

Temperature Anisotropy Map

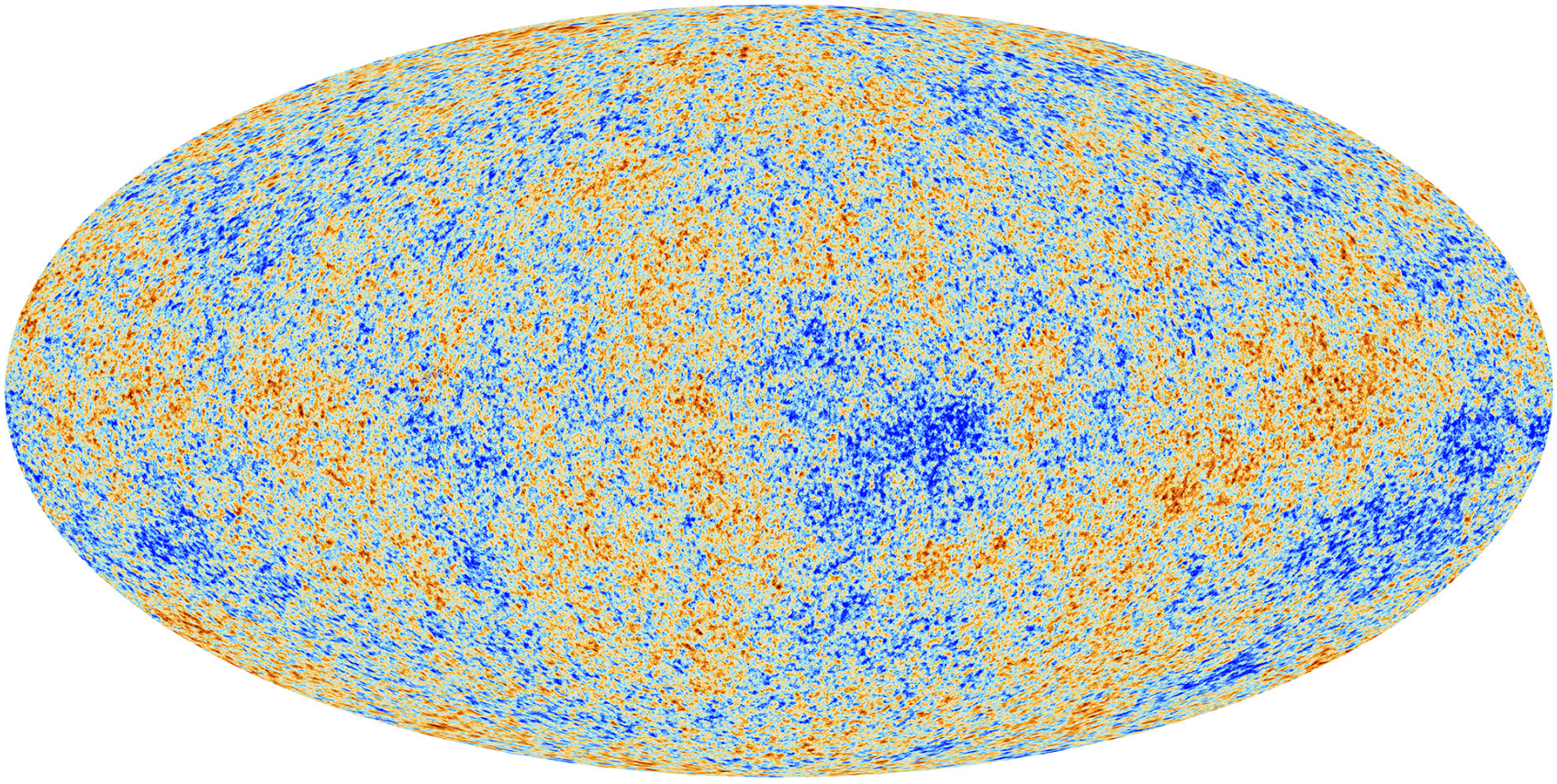

Figure: CMB Temperature Anisotropy Full Sky Map

[1] Aghanim, N. and others

Observed TT Power Spectrum

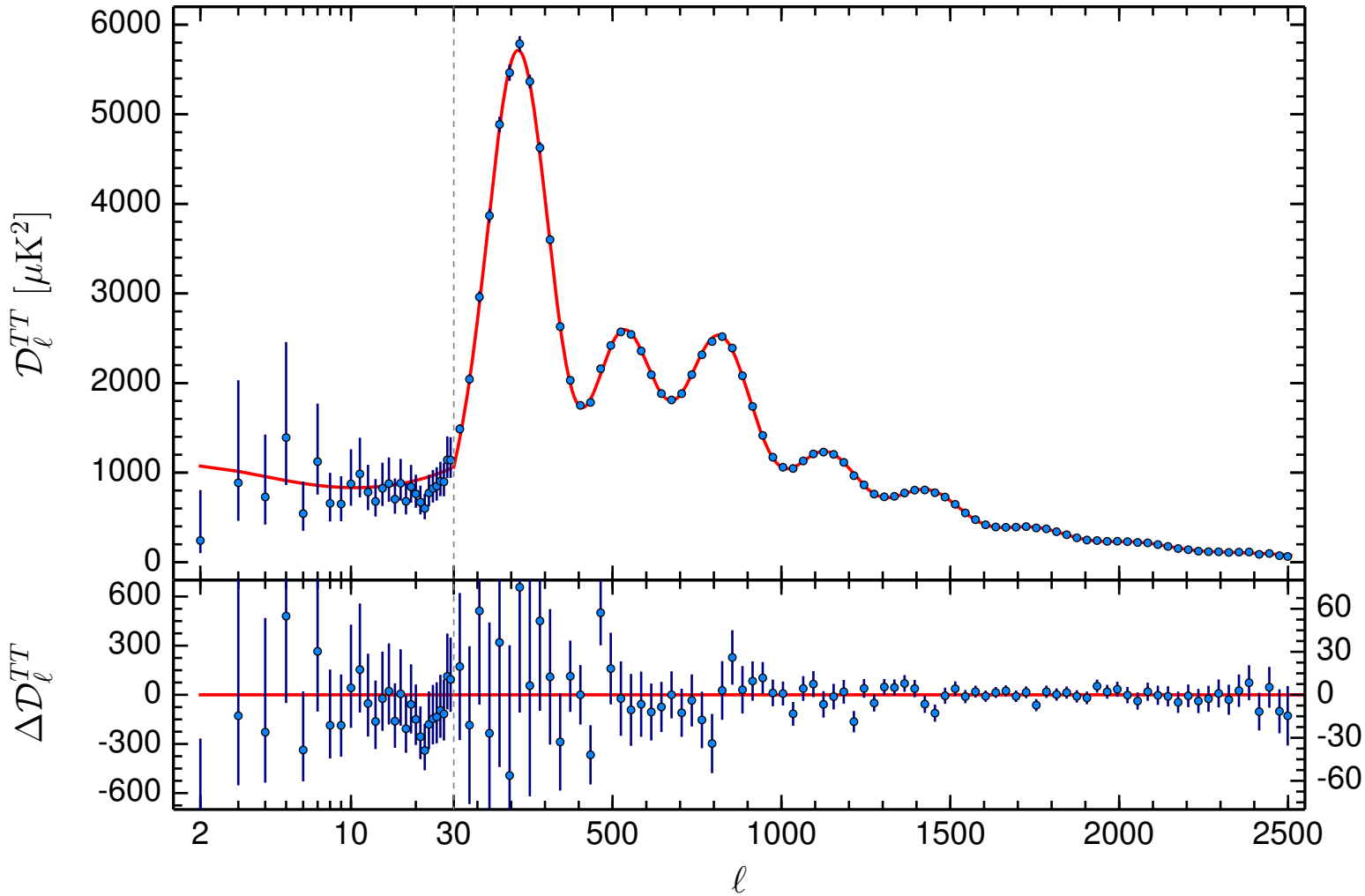

Figure: TT Power Spectrum

[1] Aghanim, N. and others

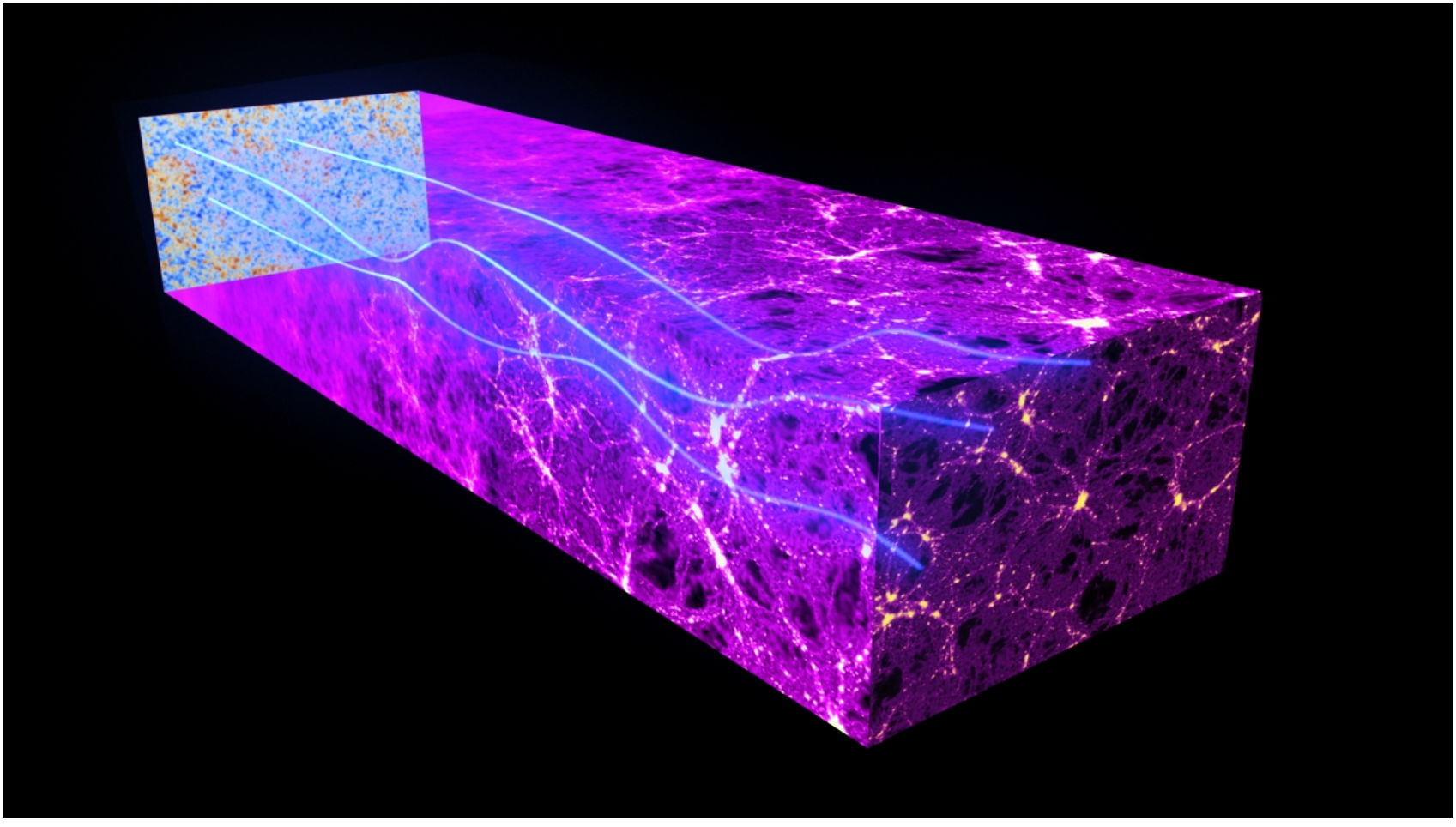

Figure: Weak Gravitational Lensing of CMB Photons

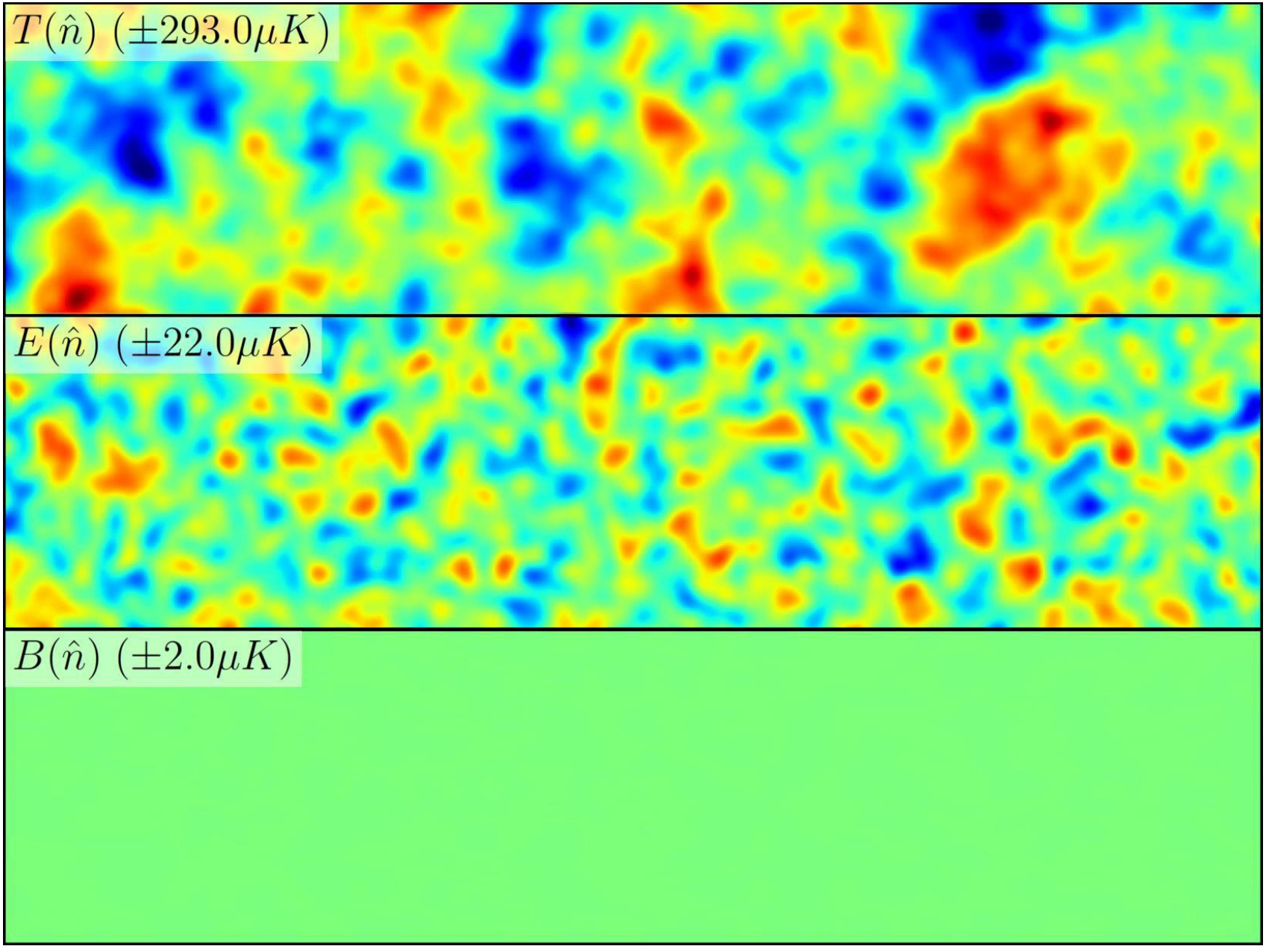

Figure: Unlensed CMB Fields

Credits : D. Hanson

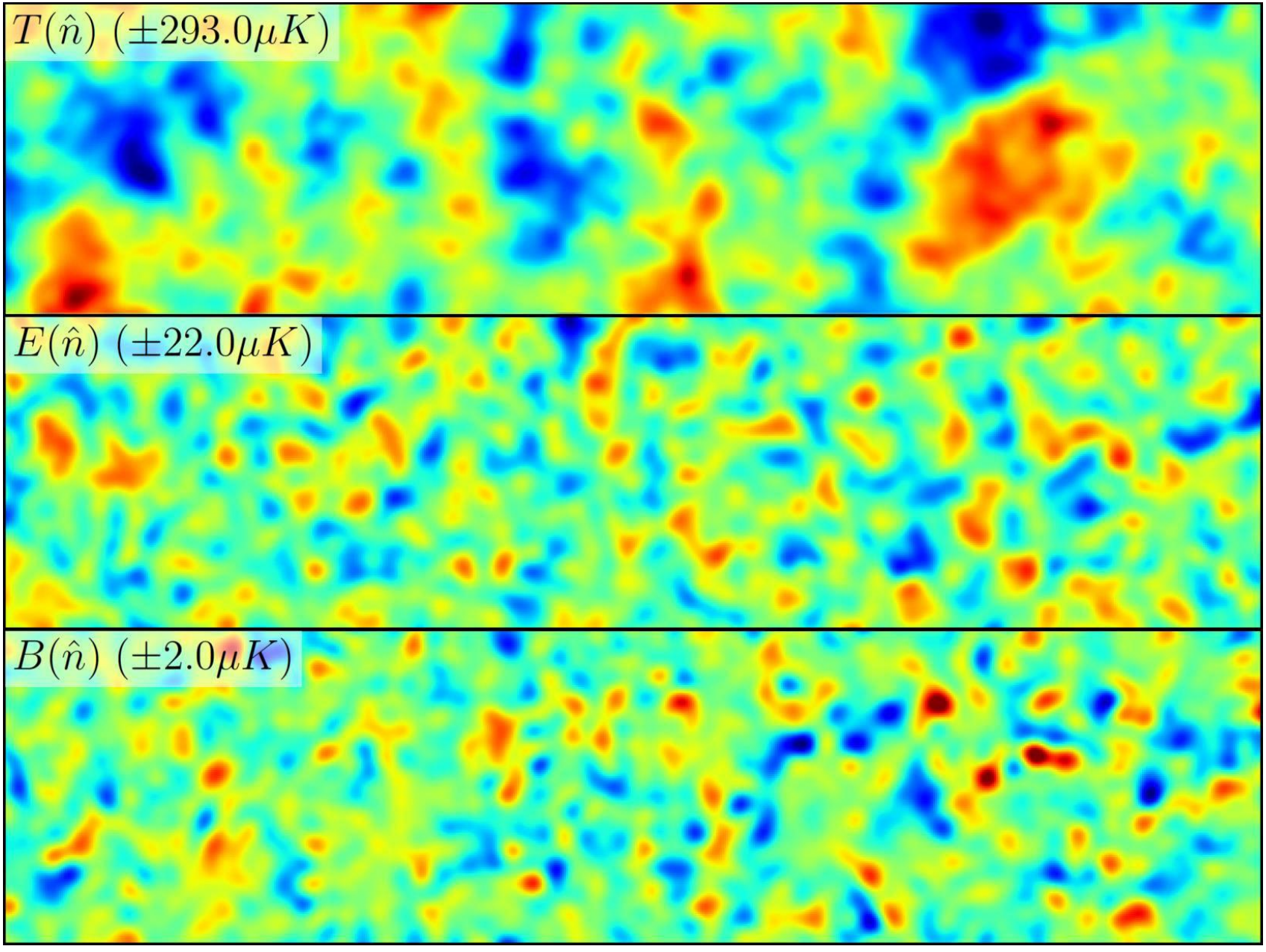

Figure: Lensed CMB Fields

Credits : D. Hanson

Formalism

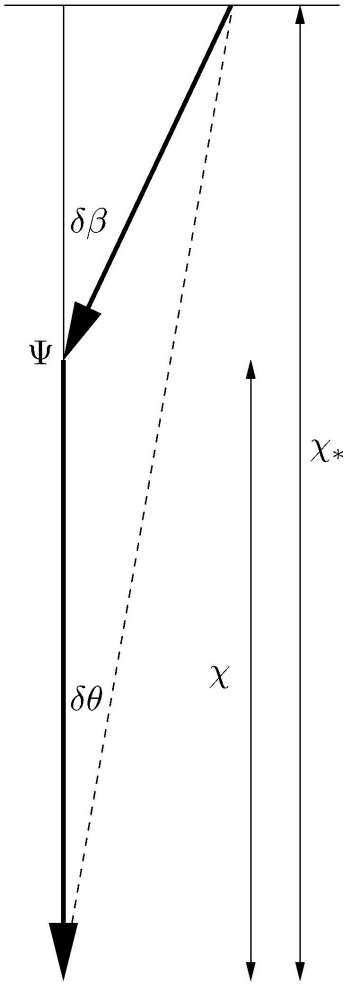

Figure: Source Remapping Due to Weak Lensing [2] Lewis and Challinor

The deflection of a photon is given by $\delta\beta = -2\delta\chi\nabla_\perp\phi$, over a small length $\delta\chi$ along the photon path.

$$f_K(\chi_* - \chi)\delta\beta = f_K(\chi_*)\delta\theta \tag{1}$$

$$\begin{aligned}\delta\theta_\chi &= \frac{f_K(\chi_* - \chi)\delta\beta}{f_K(\chi_*)} \\ &= -\frac{f_K(\chi_* - \chi)}{f_K(\chi_*)} 2\delta\chi\nabla_\perp\phi\end{aligned} \tag{2}$$

Formalism

$$\tilde{\Theta}(\hat{n}) = \Theta(\hat{n} + \vec{\alpha}) \tag{3}$$

$$\vec{\alpha} = -2 \int_0^{\chi_*} \nabla_{\hat{n}} \Phi(\chi \hat{n}; \eta_0 - \chi) \frac{f_K(\chi_* - \chi)}{f_K(\chi_*) f_K(\chi)} d\chi \tag{4}$$

$$\Phi(\chi \hat{n}; \eta_0 - \chi) = T_\Phi(k; \eta) R(k) \tag{5}$$

$$\begin{aligned} C_L^{\kappa\kappa} &= \frac{[L(L+1)]^2}{2\pi} C_L^{\phi\phi} \\ &= \frac{[L(L+1)]^2}{2\pi} 4\pi \int P_R(k) \Bigg[\int_0^{\chi_*} 2\, T_\phi(k; \eta_0 - \chi) \\ &\qquad \left(\frac{(\chi_* - \chi)}{\chi_* \chi} \right) j_L(k\chi) d\chi \Bigg]^2 \frac{dk}{k} \end{aligned}$$

Lensing Effect on Power Spectrum

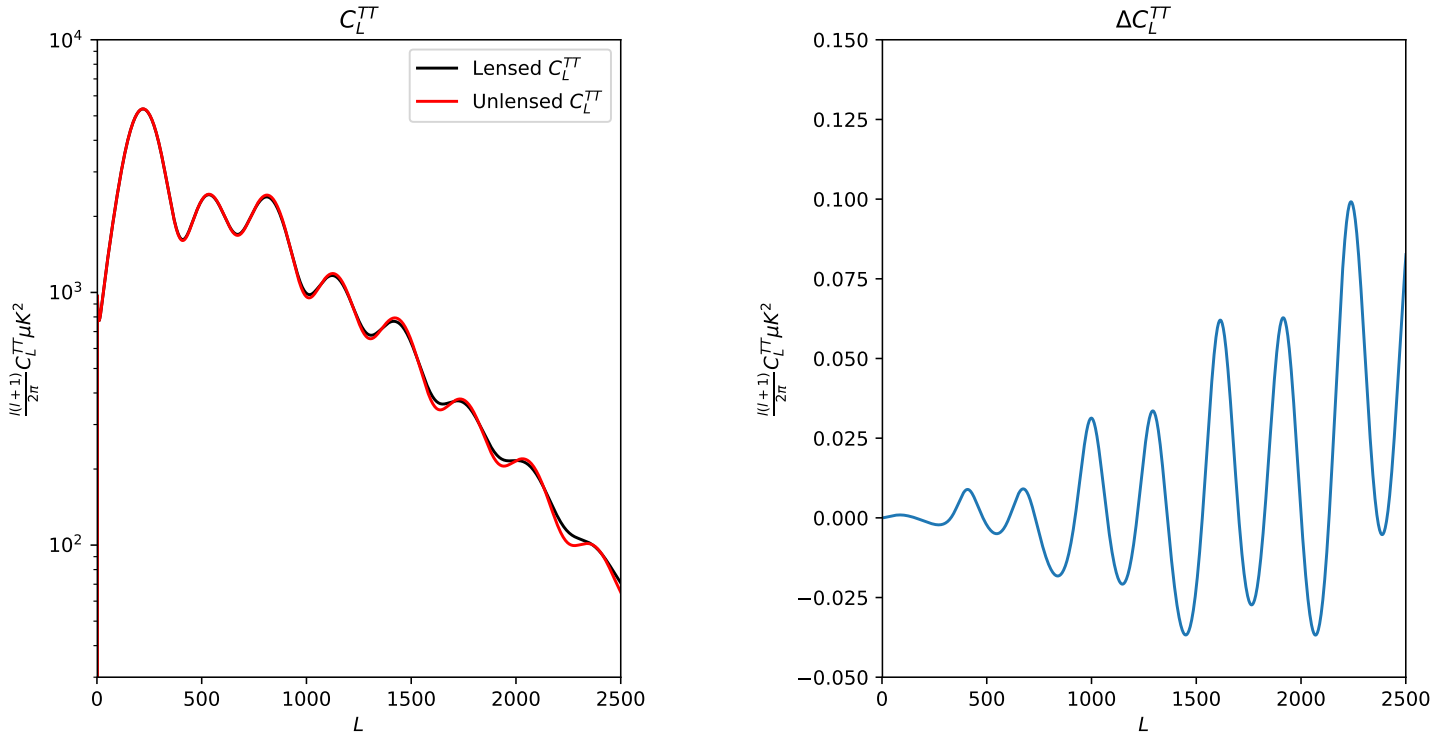

Figure: Lensed and unlensed power spectrum and the fractional change in power due to lensing at different scales. CAMB

Lensing Potential Power Spectrum

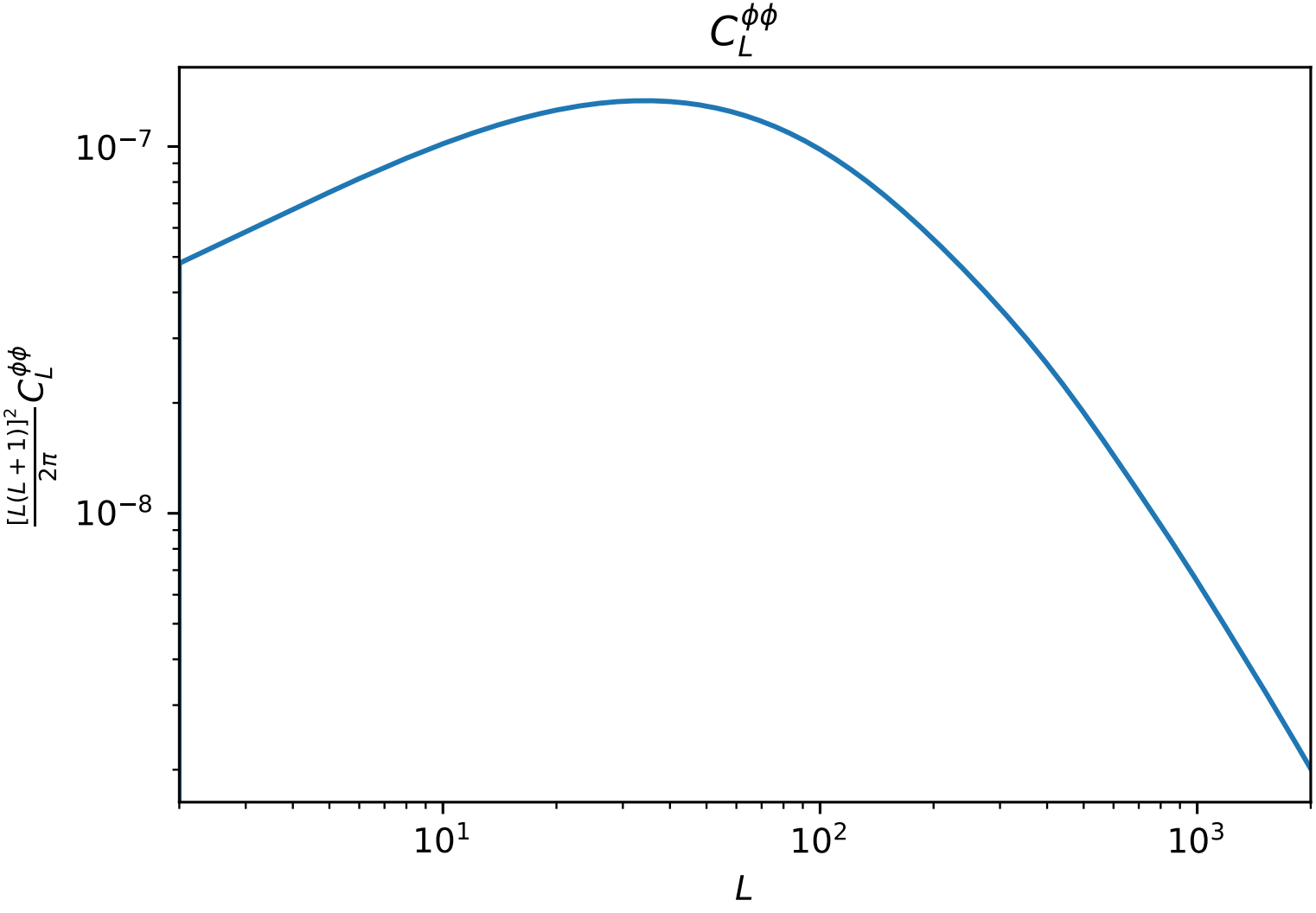

Figure: Lensing Potential Power Spectrum. CAMB

$C_L^{\phi\phi}$ Variation with neutrino mass sum $\sum m_\nu$

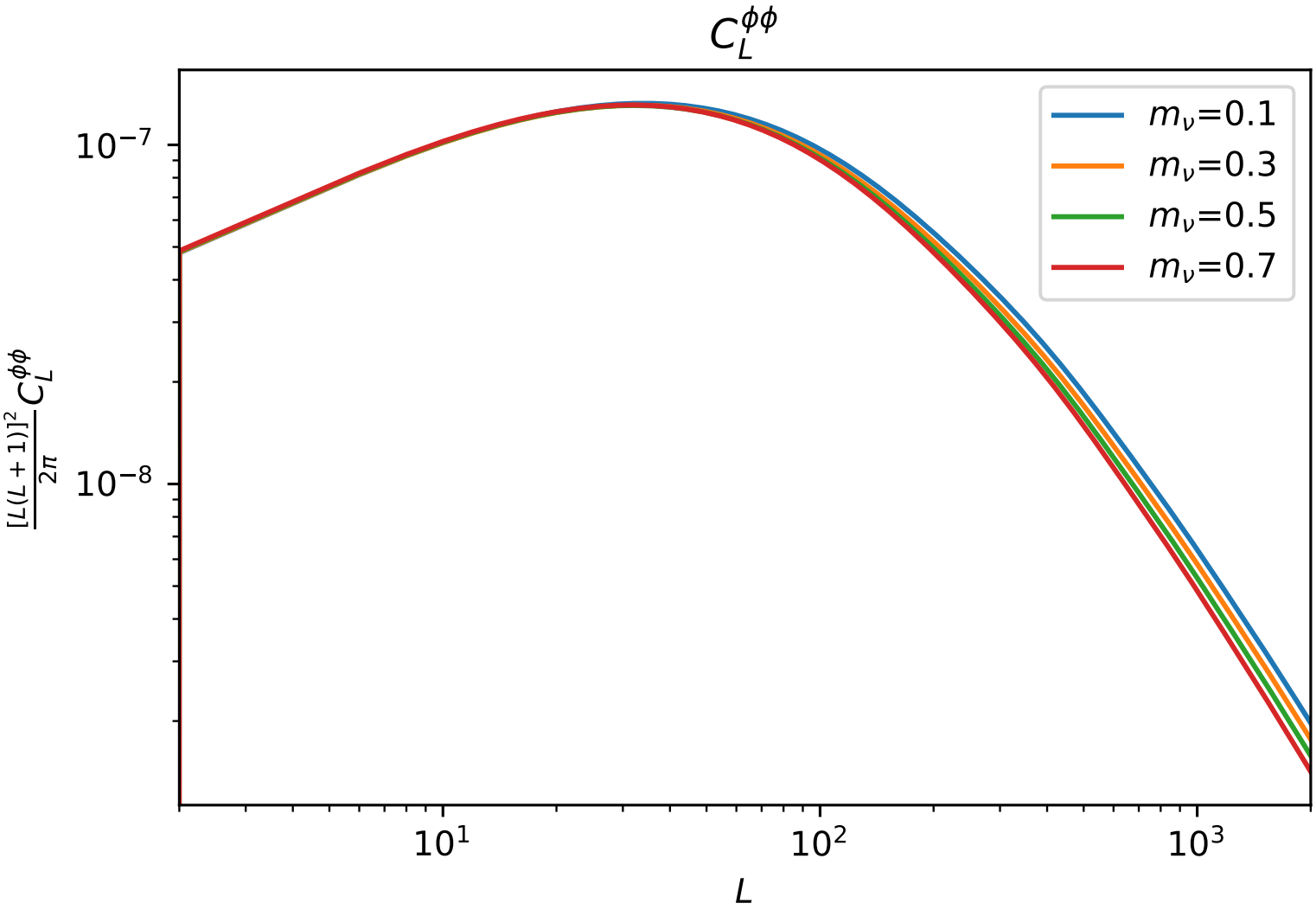

Figure: Lensing Potential Power Spectrum. CAMB

$C_L^{\phi\phi}$ Variation with DE equation of state w

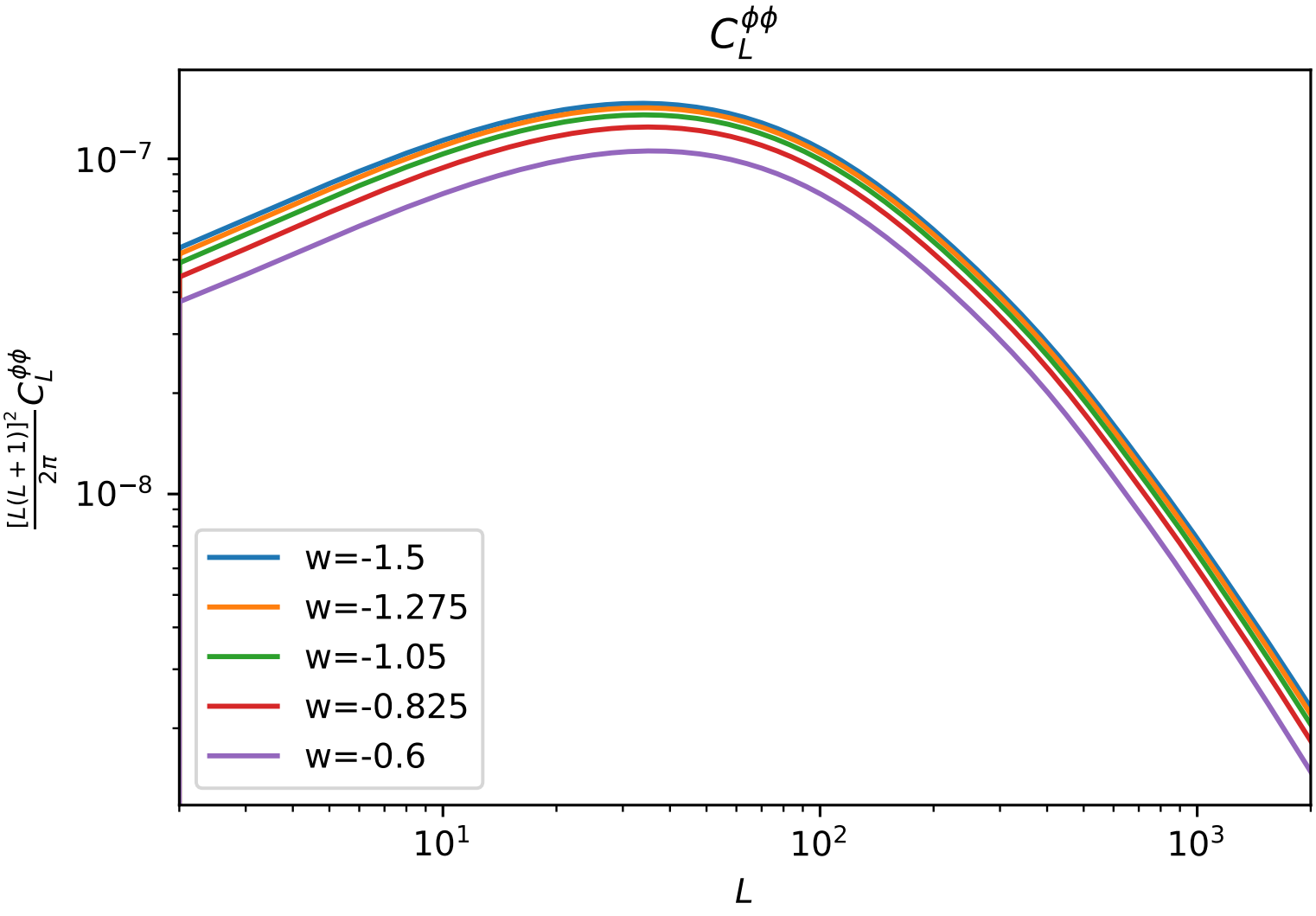

Figure: Lensing Potential Power Spectrum. CAMB

Kernel

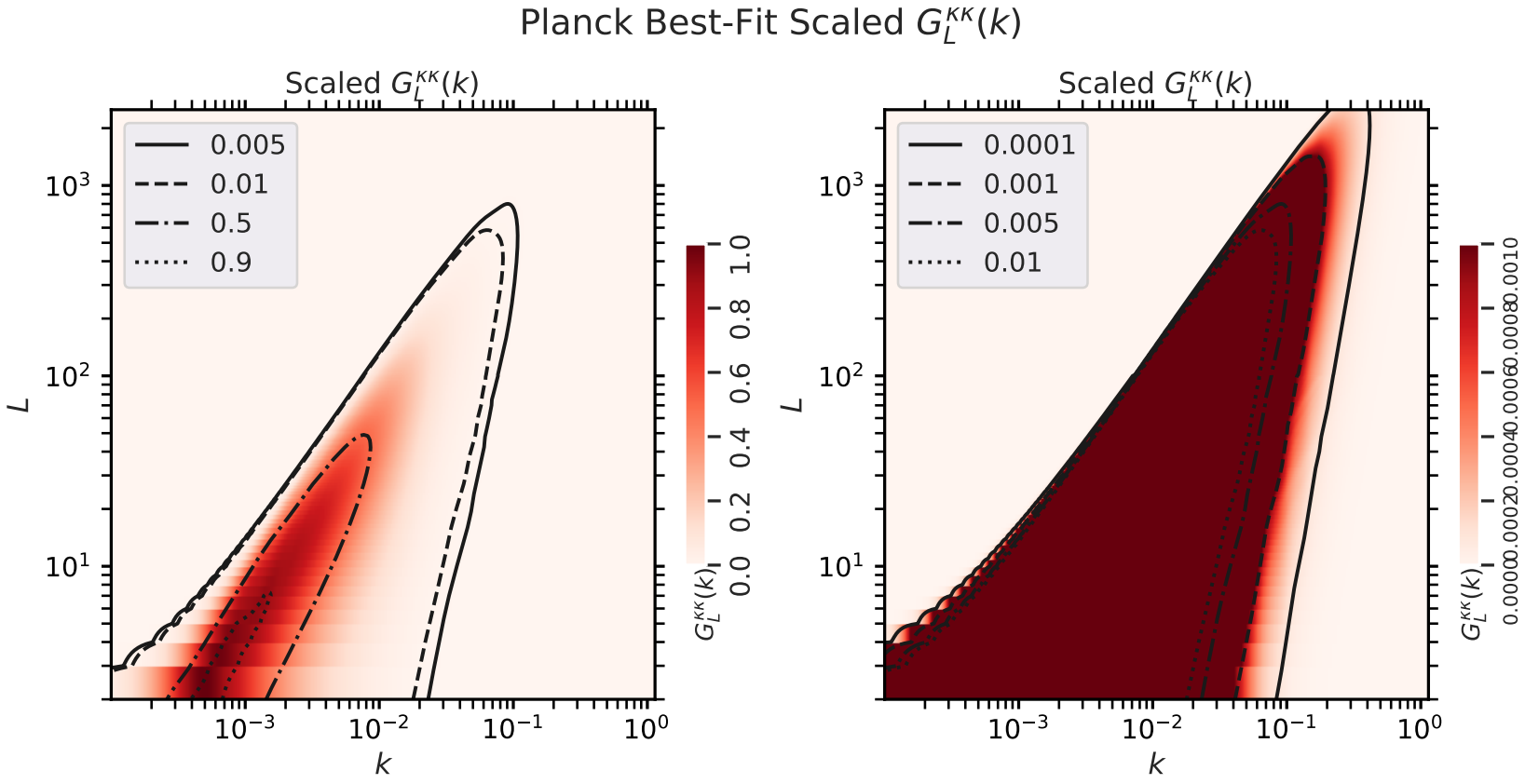

Figure: This plot shows a topdown view of the scaled transfer function given by $G_L^{\kappa\kappa}(k)/G_L^{\kappa\kappa}(k)_{max}$. The first plot shows the function with the complete power range 0 to 1 on the colorbar and 4 power level contours. The second plot shows the function in a power range 0 upto 0.001 on the colorbar with 4 power level contours.

Kernel

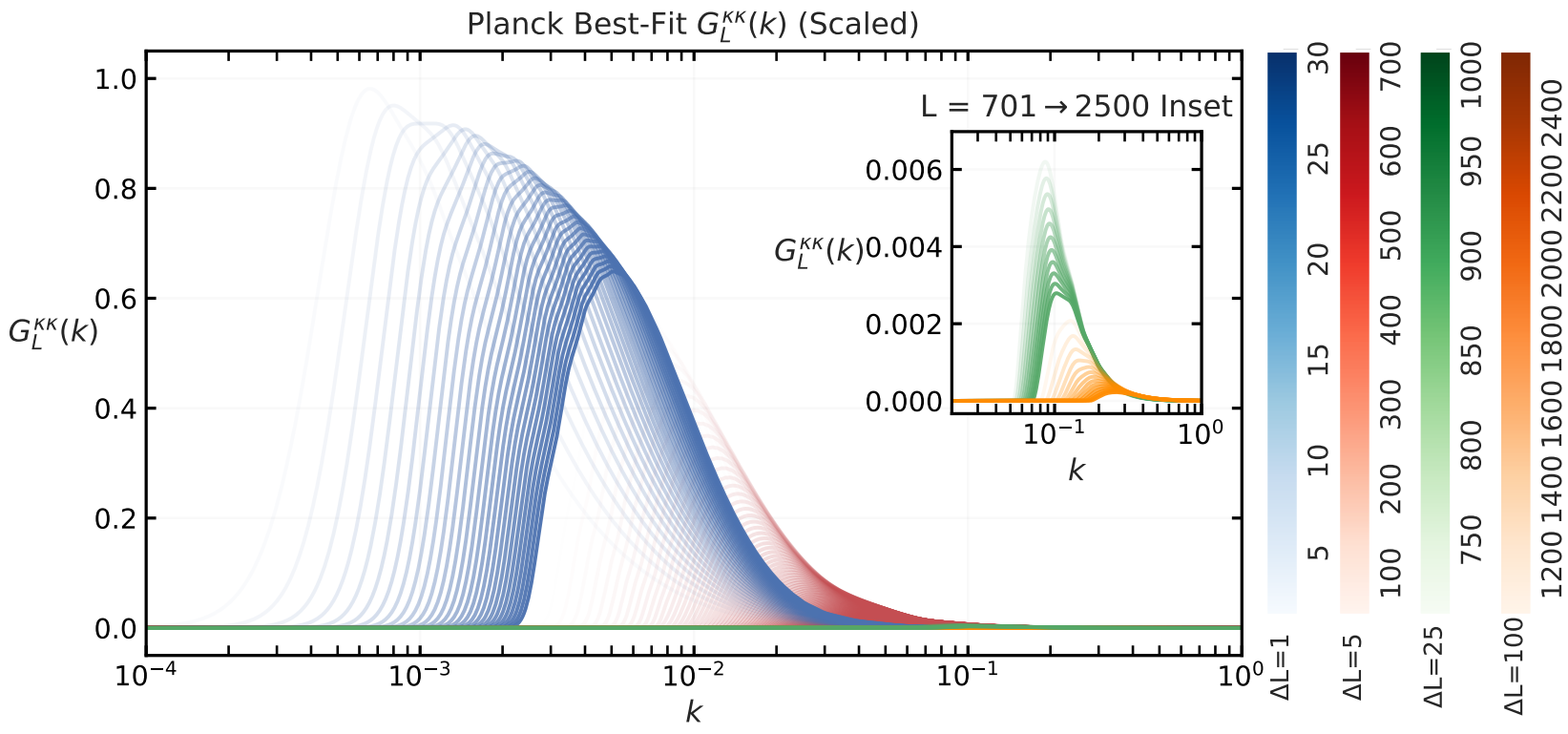

(a)

Figure: Plot a) shows the functional form of the $G_L^{\kappa\kappa}(k)$ kernel projected onto the k vs $G_L^{\kappa\kappa}(k)$ plane where L is parametrized as a color gradient within blocks of L with corresponding ΔL step sizes showing the plotted frequency of L blocks. The L blocks are roughly segemented by the relative amount of power they transfer.

Kernel

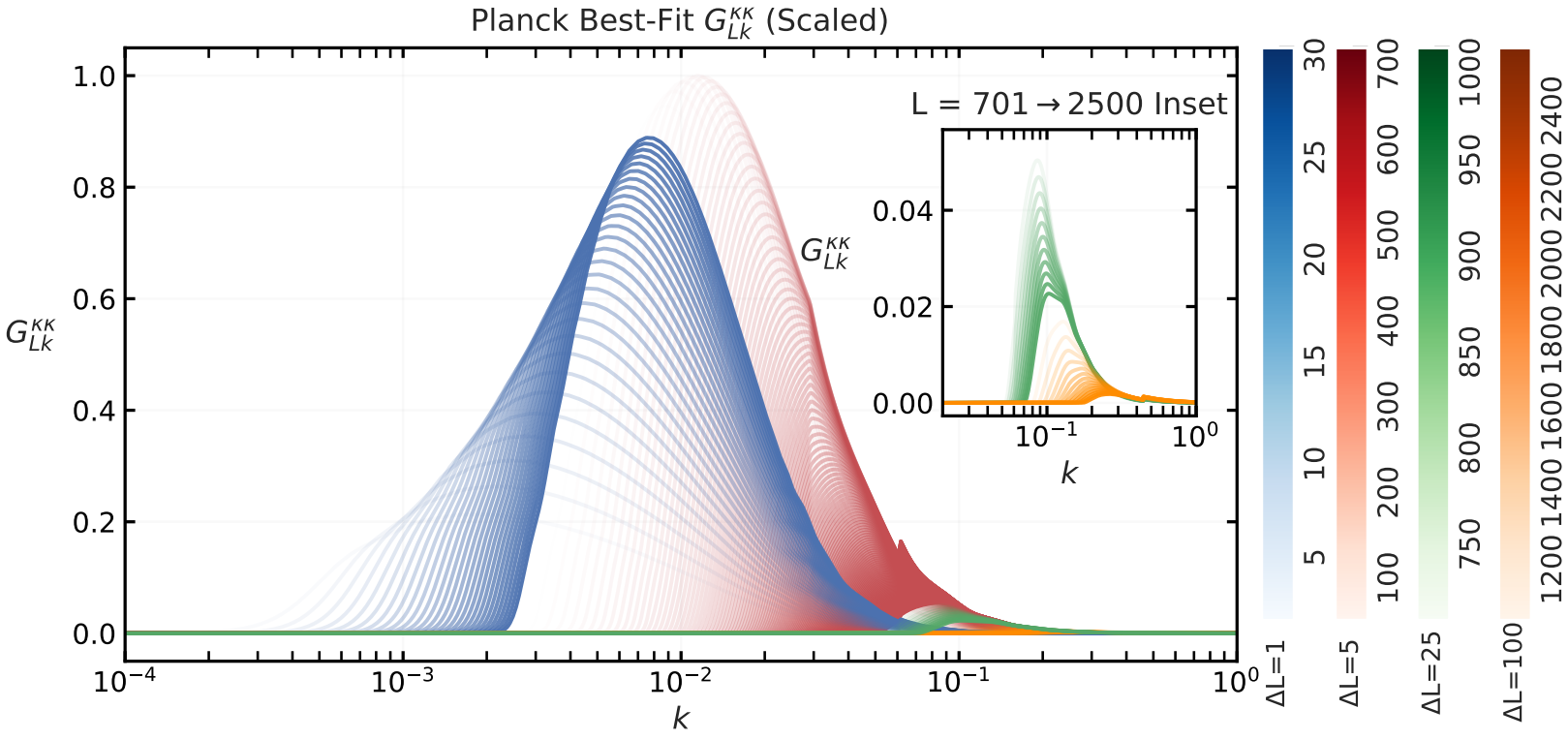

(a)

Figure: Plot b) shows the same kernel but with the numerical integration step size multiplied. $G_{Lk}^{\kappa\kappa} = G_{L}^{\kappa\kappa}(k)\Delta k$.

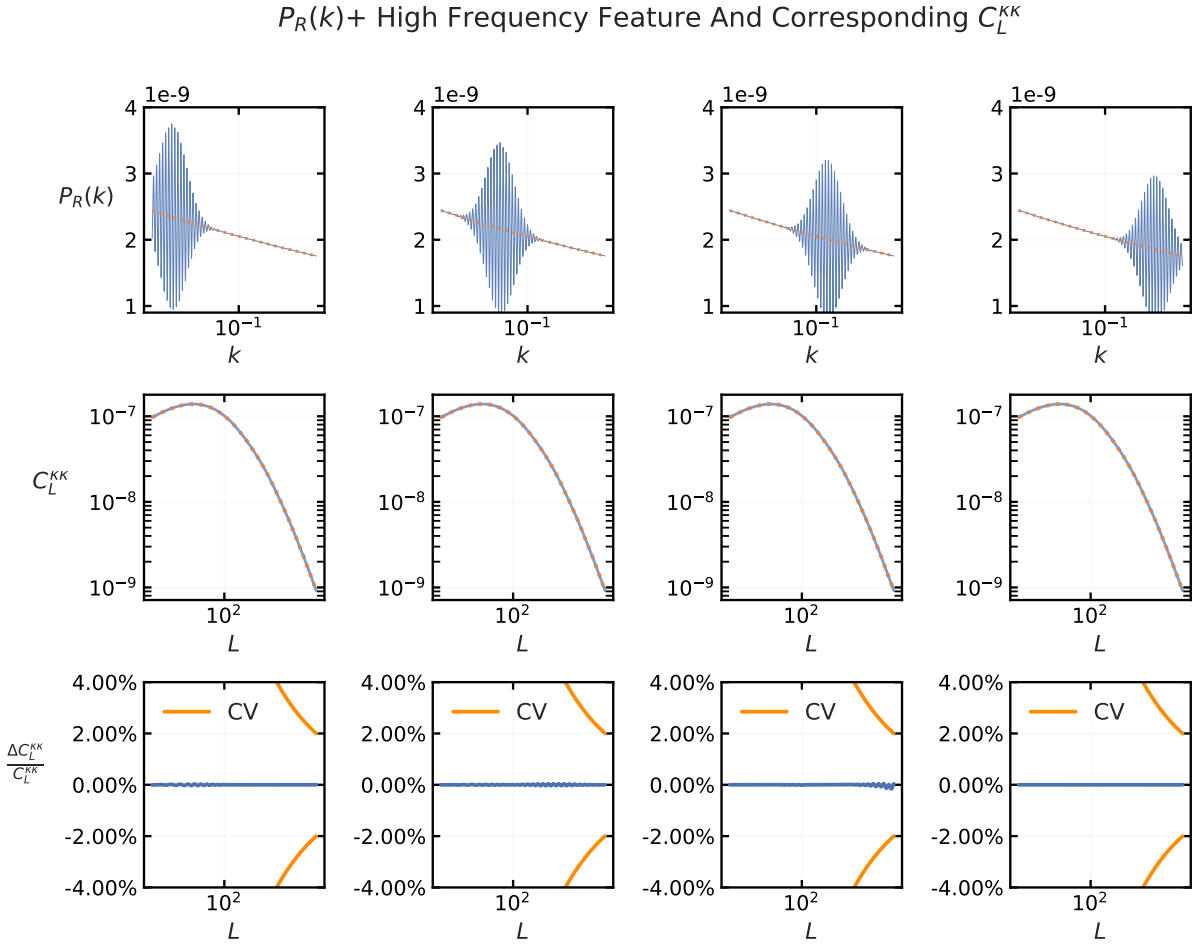

Figure: This plot shows a high frequency feature in the form of a wavepacket (blue line) superimposed on a power law (orange dash) PPS, plotted on the top row. $C_L^{\kappa\kappa}$ from power law (orange dash) vs wavepacket superimposed PPS (blue line) is plotted in the mid row. Percent difference between the two $C_L^{\kappa\kappa}$ in blue in the bottom row, compared to cosmic variance in orange. The k ranges from 10^{-5} to 10 and L ranges from 2 to 2500. The feature moves across k space from left to right.

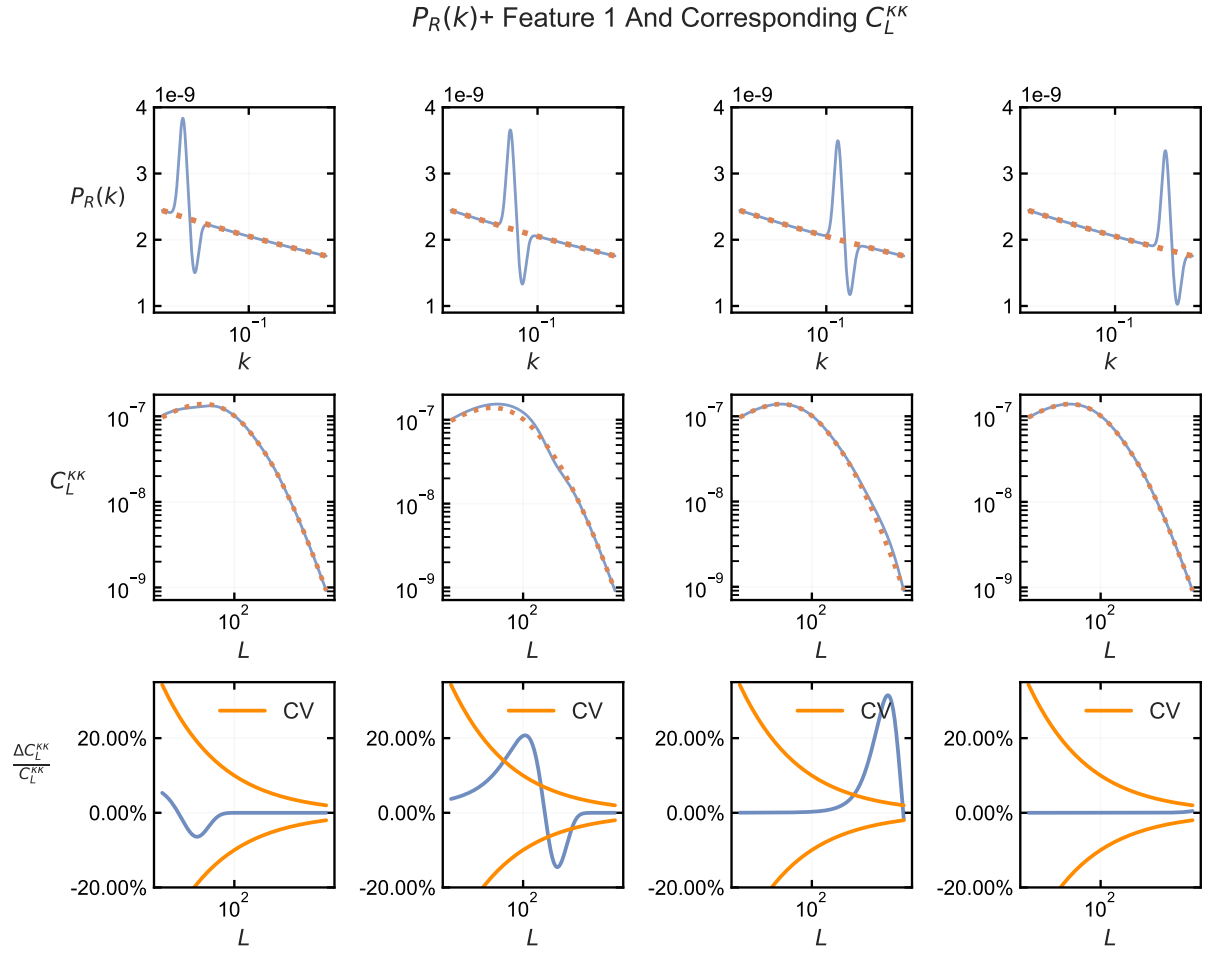

Figure: This plot shows a low frequency Feature 1 (blue line), plotted on the top row superimposed with a power law (orange dash) PPS. Corresponding $C_L^{\kappa\kappa}$ from Feature 1 (blue line) based vs power law (orange dash) PPS in the mid row. Percent power difference in $C_L^{\kappa\kappa}$ (blue line) shown in the bottom row vs cosmic variance (orange line). The k ranges from 5×10^{-4} to 10 and L ranges from 8 to 2500. Feature 1 moves across k space from left to right.

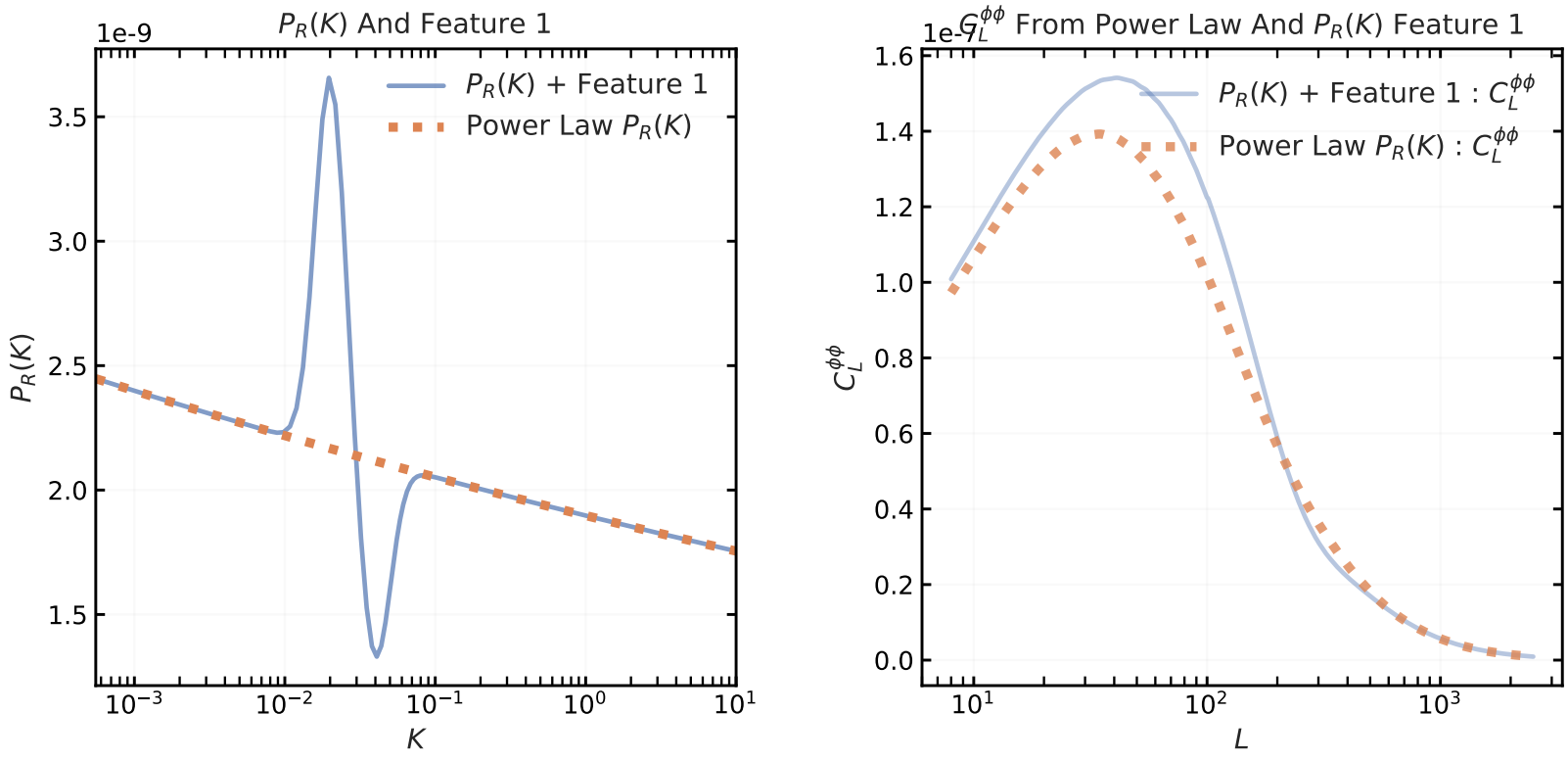

Figure: a) Plots a low frequency feature, Feature 1, superimposed on the power law $P_R(k)$. b) Plots the corresponding $C_L^{\kappa\kappa}$ from $P_R(k)$ with and without Feature 1.

Reconstruction Algorithm : Richardson-Lucy

$$P_k^{(i+1)} = P_k^{(i)} \left[1 + \sum_L \tilde{G}_{Lk}^{\kappa\kappa} \left(\frac{\hat{C}_L^{\kappa\kappa}}{C_L^{\kappa\kappa(i)}} - 1 \right) \tanh^2 \left([\hat{C}_L^{\kappa\kappa} - C_L^{\kappa\kappa(i)}] \Sigma_{LL'}^{-1} \right.\right.$$
$$\left.\left. [\hat{C}_{L'}^{\kappa\kappa} - C_{L'}^{\kappa\kappa(i)}]^T \right) \right]$$
$$= P_k^{(i)} \left[1 + \sum_L \tilde{G}_{Lk}^{\kappa\kappa} \left(\frac{\hat{C}_L^{\kappa\kappa}}{C_L^{\kappa\kappa(i)}} - 1 \right) \tanh^2 \left(\frac{\hat{C}_L^{\kappa\kappa} - C_L^{\kappa\kappa(i)}}{\hat{\sigma}_L} \right)^2 \right]$$

$\tilde{G}_{Lk}^{\kappa\kappa}$: Discretized Kernel normalised over L

$\hat{C}_L^{\kappa\kappa}$: Data $C_L^{\kappa\kappa}$

Σ^{-1} : Error covariance matric of the data $\hat{C}_L^{\kappa\kappa}$

$$C_L^{\kappa\kappa(i)} = \sum_k G_{Lk}^{\kappa\kappa} P_k^{(i)} \tag{6}$$

[3]

Reconstruction Initial Guess Sensitivity

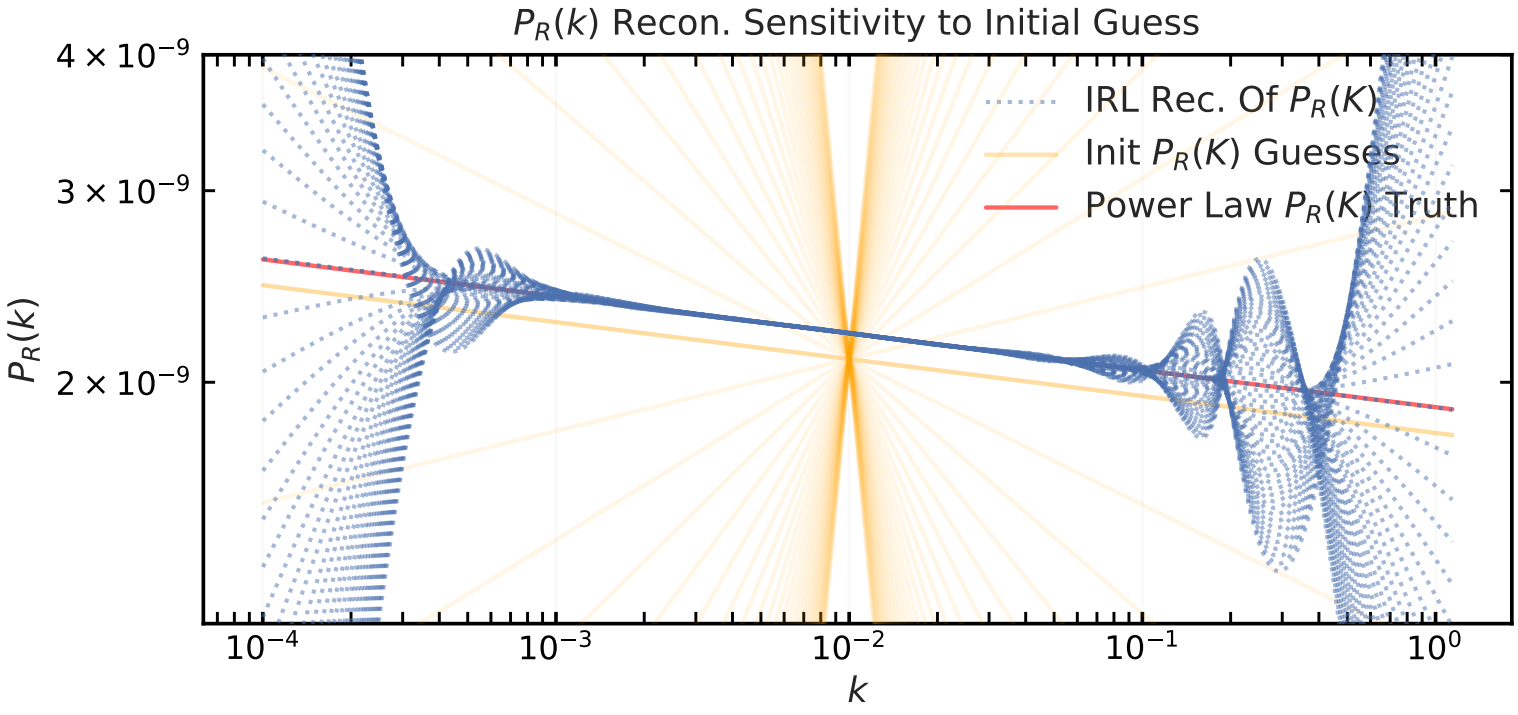

(a)

Figure: Figure a) shows the reconstructed $P_R(k)$ in blue dashed lines, given different initial guesses $P_R(k)^{(i=0)}$ in yellow lines varying by slope n_s. The red lines shows the original injected power spectrum $P_R(K)$.

Reconstruction Initial Guess Sensitivity

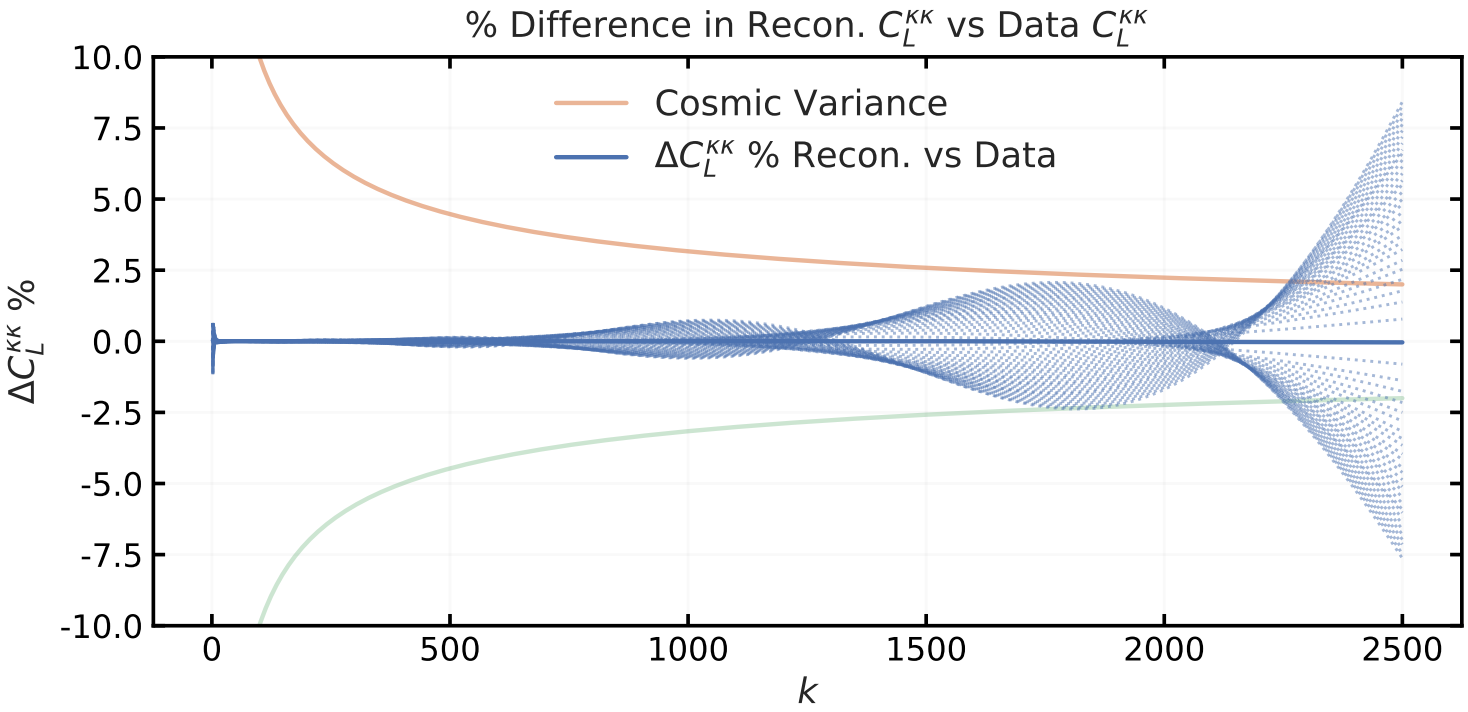

(a)

Figure: Figure b) shows the relative % difference in the reconstructed $\hat{C}_L^{\kappa\kappa}$ and the input data $C_L^{\kappa\kappa}$.

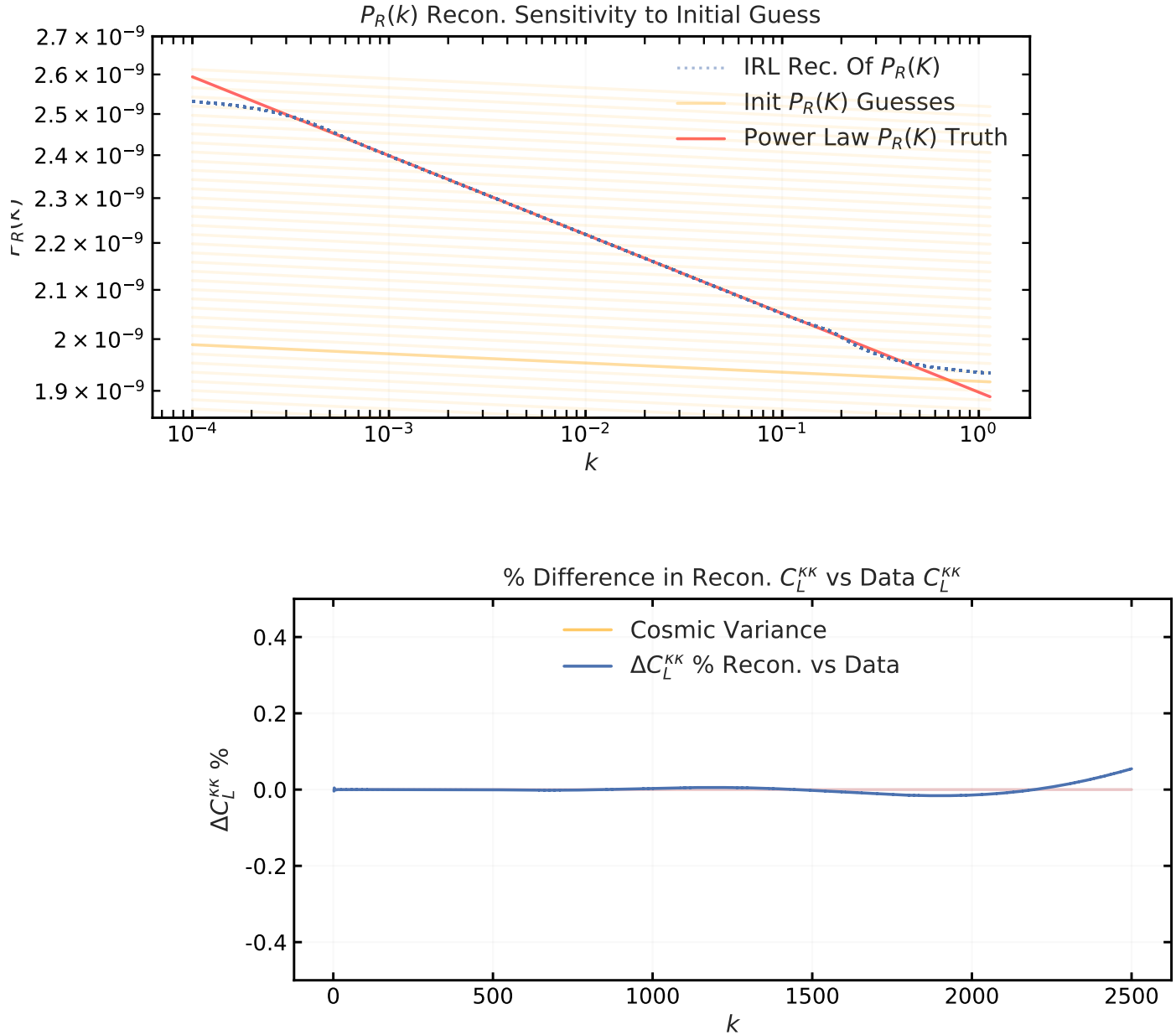

Figure: Figure a) shows the reconstructed $P_R(k)$ in blue dashed lines, given different initial guesses $P_R(k)^{(i=0)}$ in yellow lines varying by intercept $k*$ for a given slope

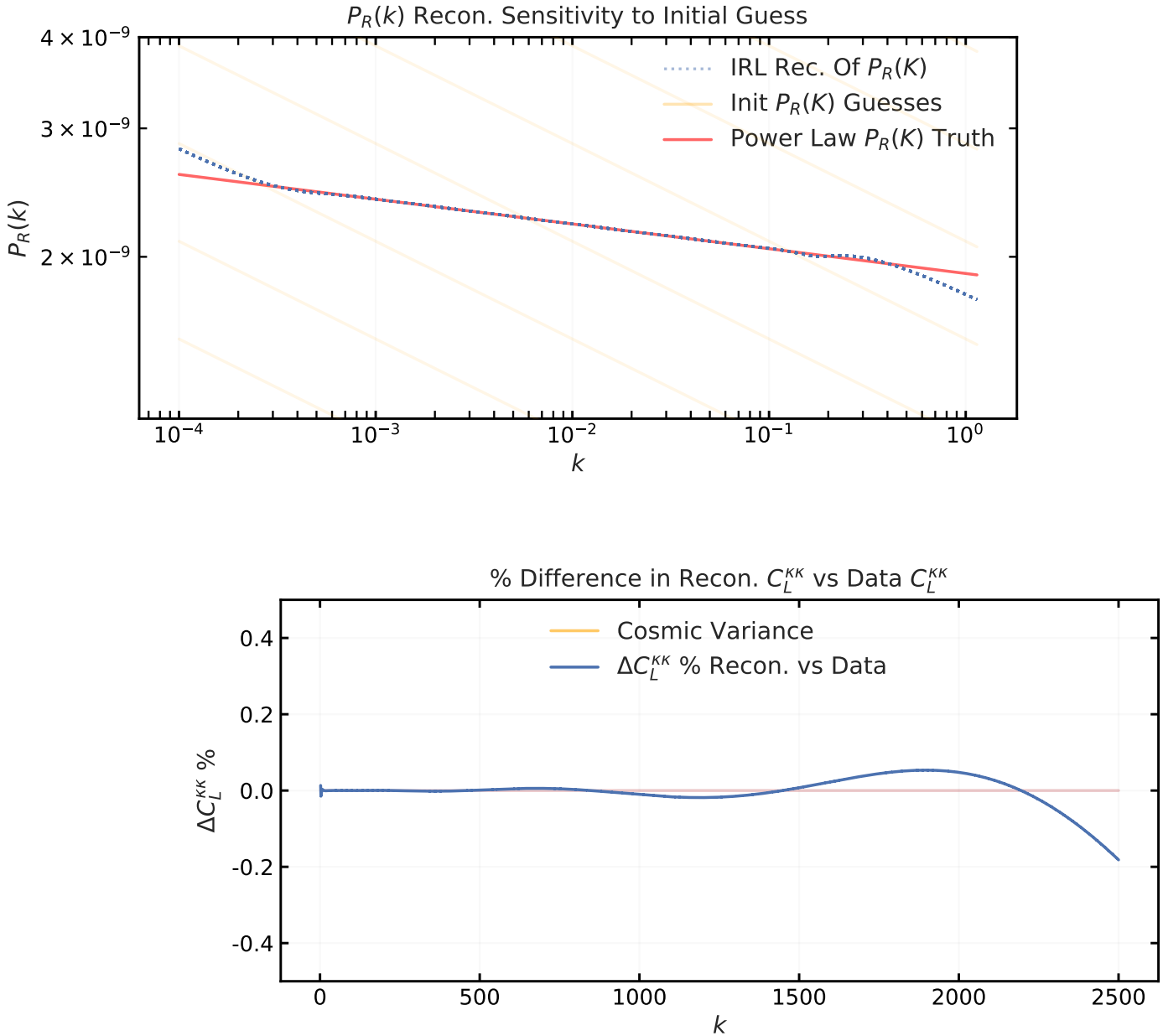

Figure: Figure a) shows the reconstructed $P_R(k)$ in blue dashed lines, given different initial guesses $P_R(k)^{(i=0)}$ in yellow lines varying by intercept $k*$ for a given slope

Input Simulation Data

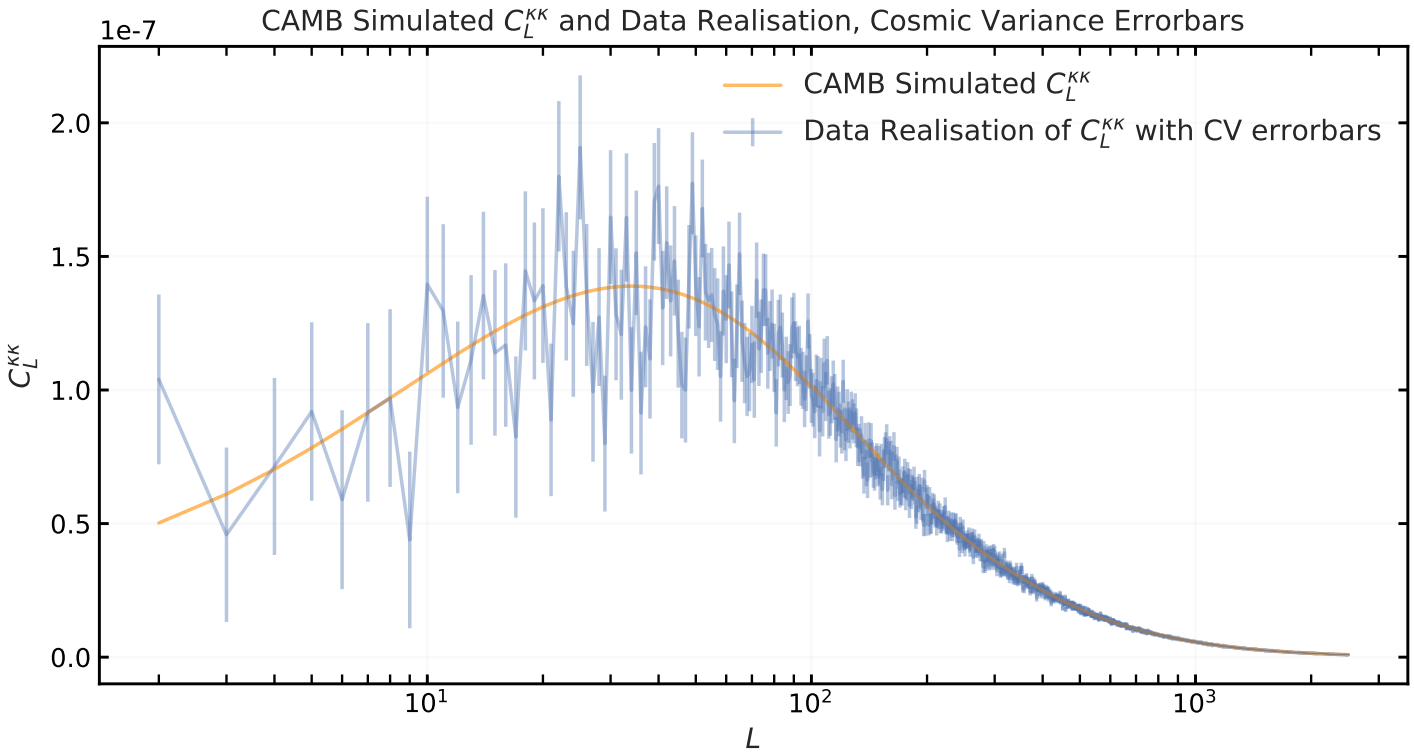

Figure: Plot of the CAMB simulated $C_L^{\kappa\kappa}$ in Orange and the data realisation by treating each $C_L^{\kappa\kappa}$ as a Gaussian random sample based on cosmic variance error bars, in blue.

$C_L^{\kappa\kappa}$ Mission Data

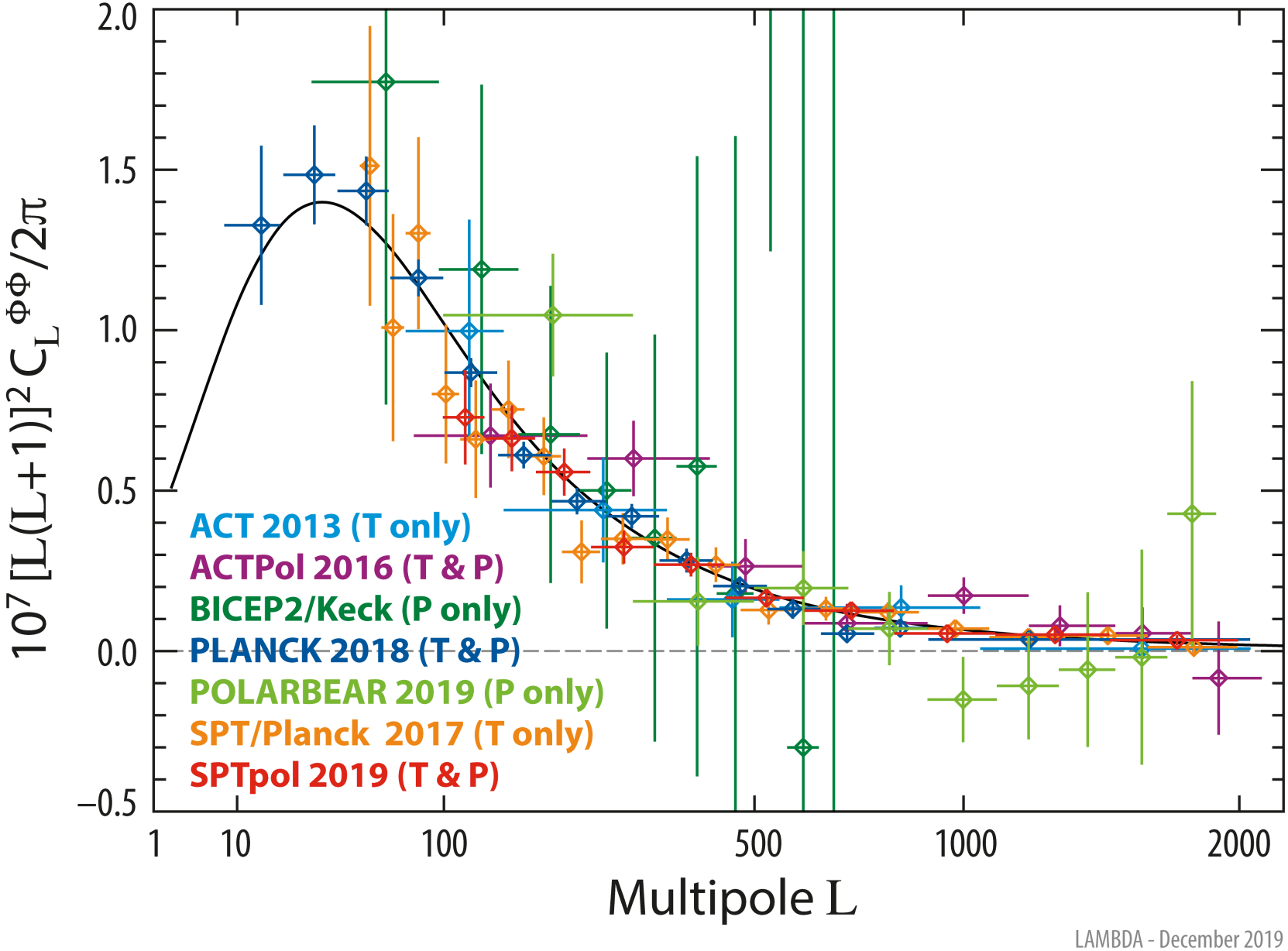

Figure: Plot of the $C_L^{\kappa\kappa}$ from various missions.

Covariance Accuracy

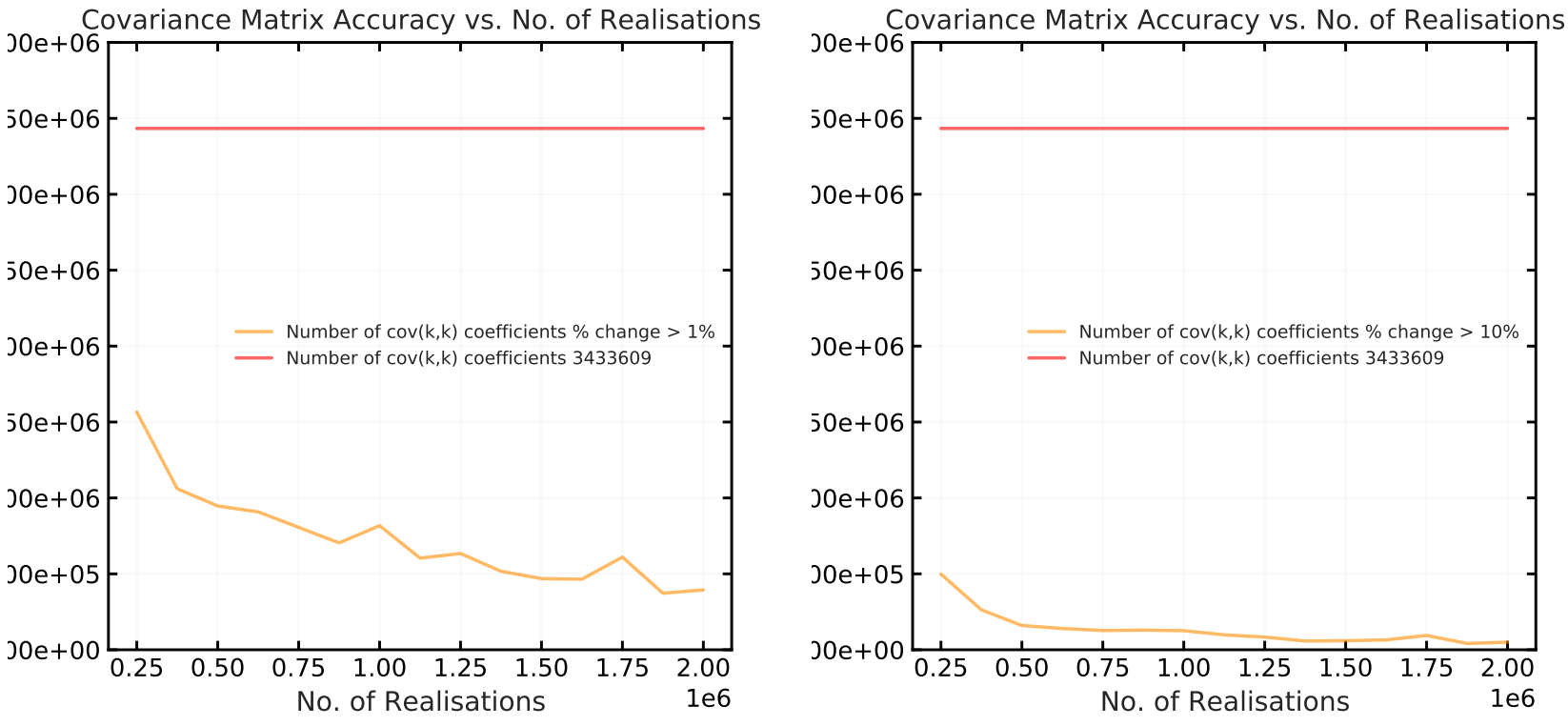

Figure: a) Plots the number of $\Sigma_{kk'}$ coefficients that exceed a 1% relative error change with respect to the previous realisation set, vs the realisation number set. We see that by 2×10^6 number of realisations, the accuracy saturates. Similarly the plot b) plots the same but at 10% accuracy threshold, showing similar saturation.

$P_R(k)$ Reconstruction

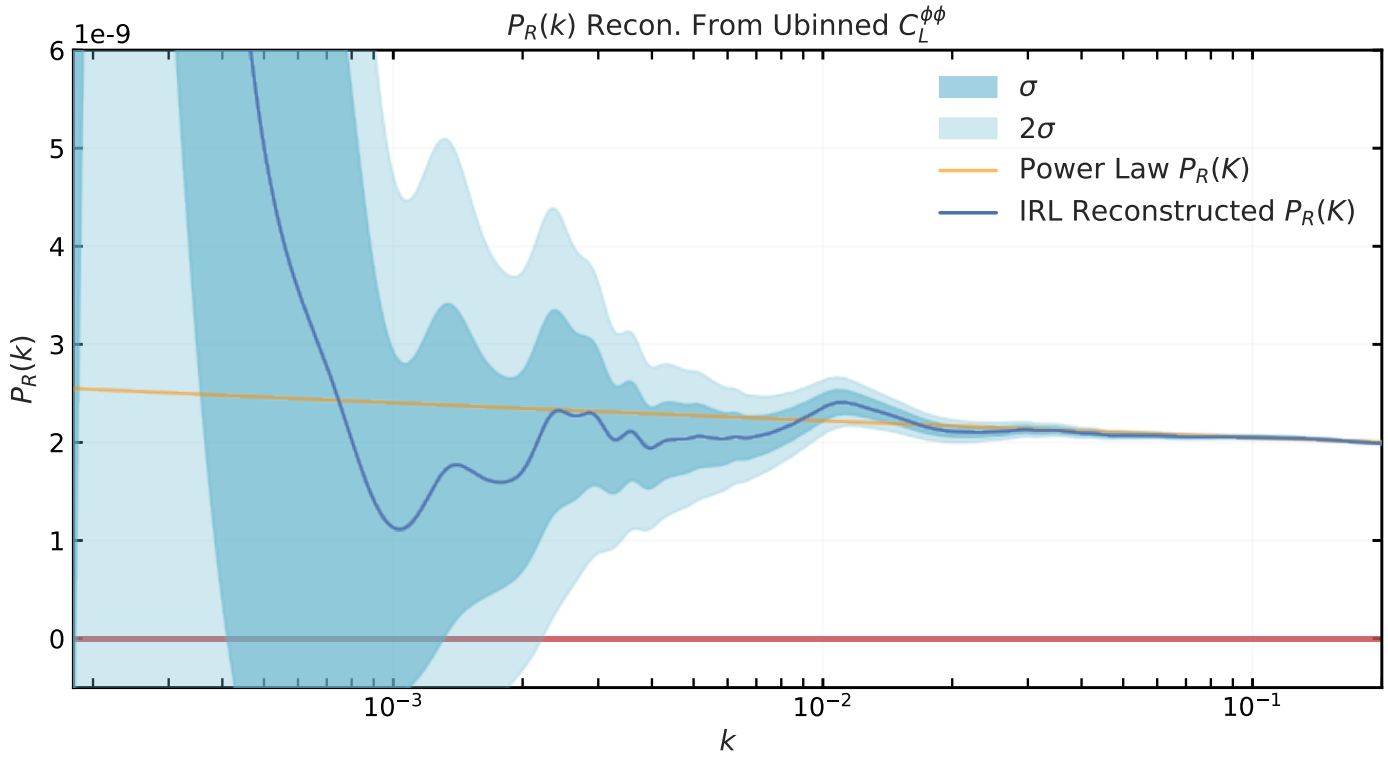

Figure: Plot of the reconstructed $P_R(k)$ (Blue) with $1\sigma, 2\sigma$ bands from 2×10^6 data realisations with cosmic variance error, overplotted on the fiducial Power Law $P_R(k)$ (Orange).

$P_R(k)$ Reconstructed $C_L^{\kappa\kappa}$

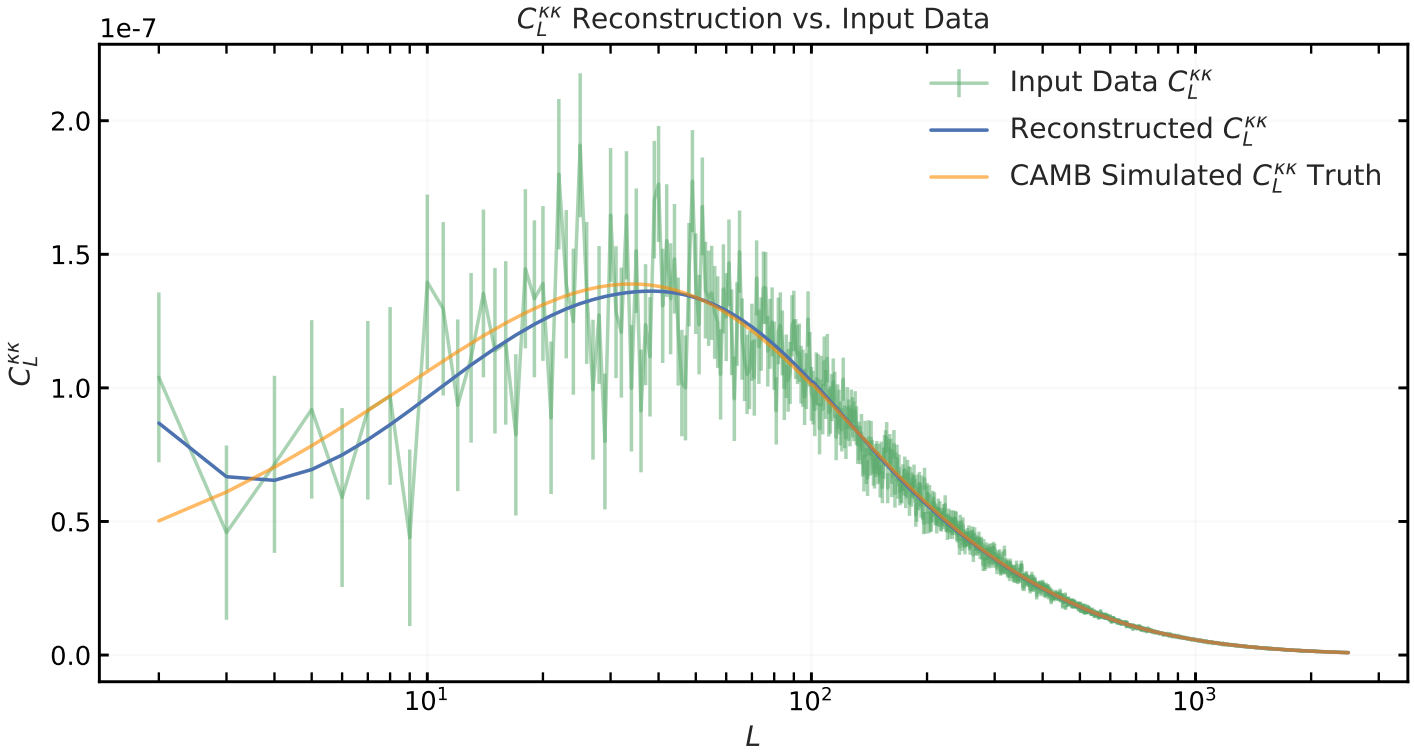

Figure: Reconstructed $C_L^{\kappa\kappa}$ in Blue plotted over the fiducial CAMB $C_L^{\kappa\kappa}$ in Orange and the input data realisation in Green.

$P_R(k)$ and $C_L^{\kappa\kappa}$ Reconstruction Error

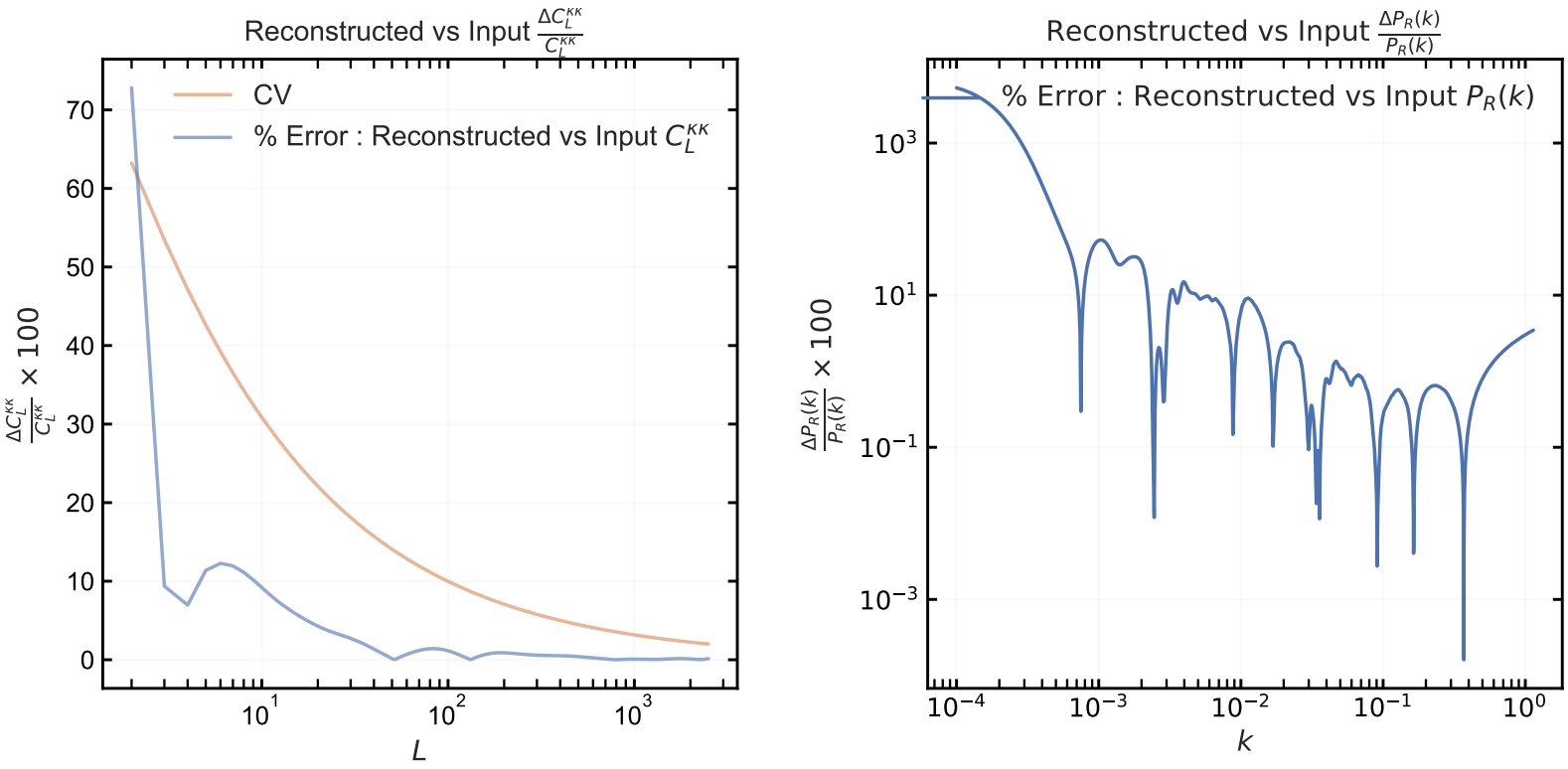

Figure: The two figures show the relative % error between the reconstructed $C_L^{\kappa\kappa}$ vs data realisation $C_L^{\kappa\kappa}$, and the reconstructed $P_R(k)$ vs input Power Law $P_R(k)$

Reconstructed $P_R(k)$ Covariance Matrix

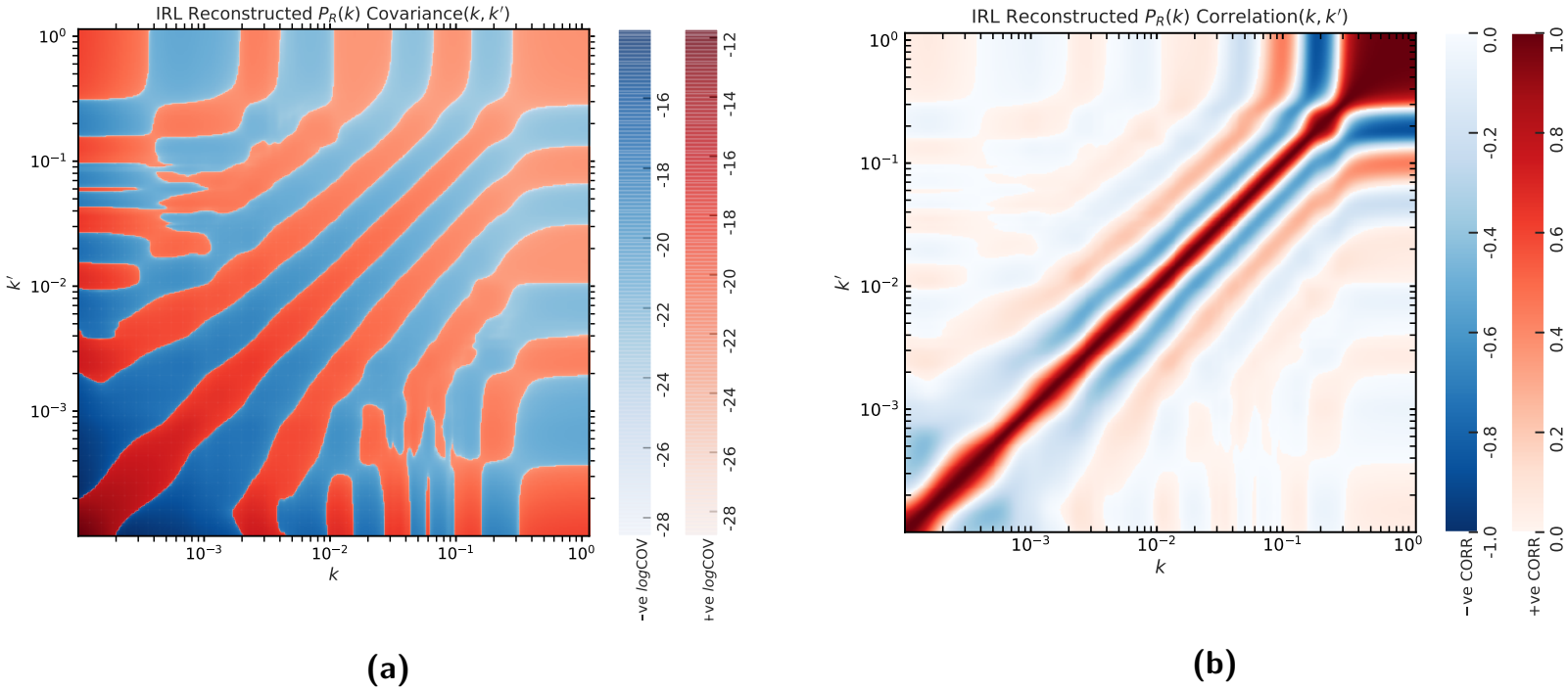

(a) **(b)**

Figure: a) is a plot of the $\Sigma_{kk'}$ from the reconstructed $P_R(k)$. Reds and Blues denote $\pm \log_{10} \Sigma_{kk'}$ respectively. The plot b) plots the correlations matrix $\rho_{kk'}$ with the Reds, Blues being the $\pm 0 \rightarrow 1$ range respectively.

$P_R(k)$ Covariance Singularity Test

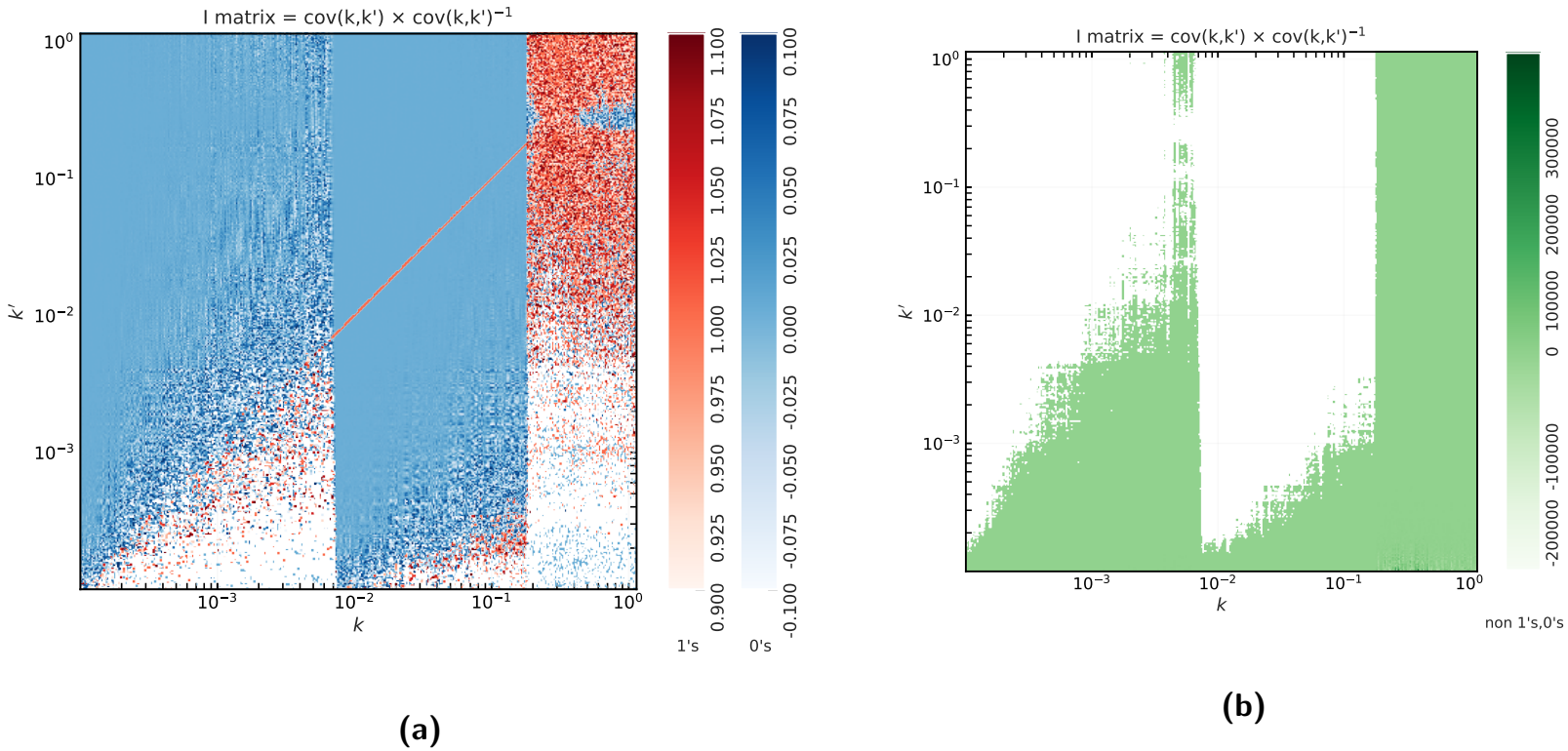

(a) **(b)**

Figure: a) Plots the $\Sigma_{kk'} \times \Sigma^{-1}_{kk'}$ with Reds, Blues being 1 ± 0.1, 0 ± 0.1 respectively . The plot b) shows the same matrix but for the non 1 ± 0.1,0 ± 0.1 terms.

Covariance Accuracy

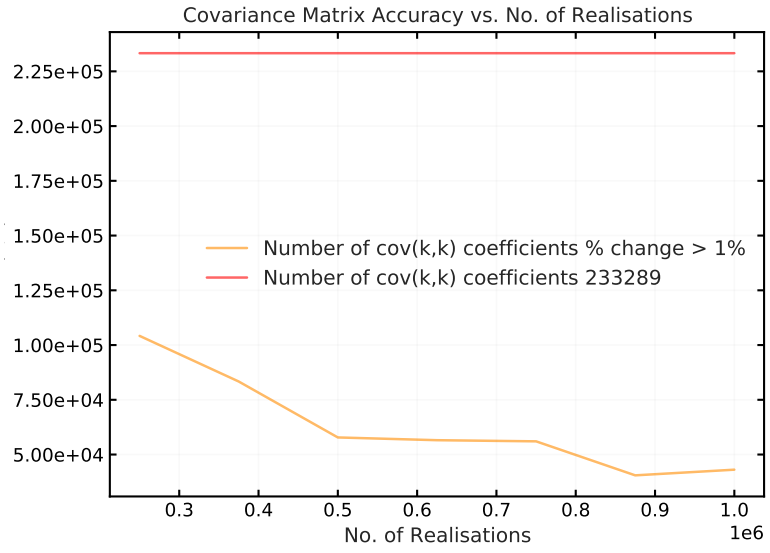

(a)

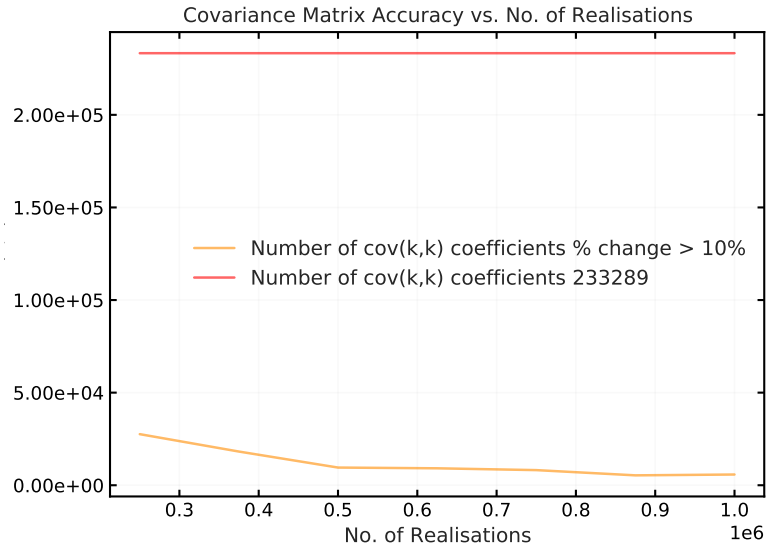

(b)

Figure: a) Plots the number of $\Sigma_{kk'}$ coefficients that exceed a 1% relative error change with respect to the previous realisation set, vs the realisation number set. We see that by 2×10^6 number of realisations, the accuracy saturates. Similarly the plot b) plots the same but at 10% accuracy threshold, showing similar saturation.

Sparse $P_R(k)$ Reconstruction

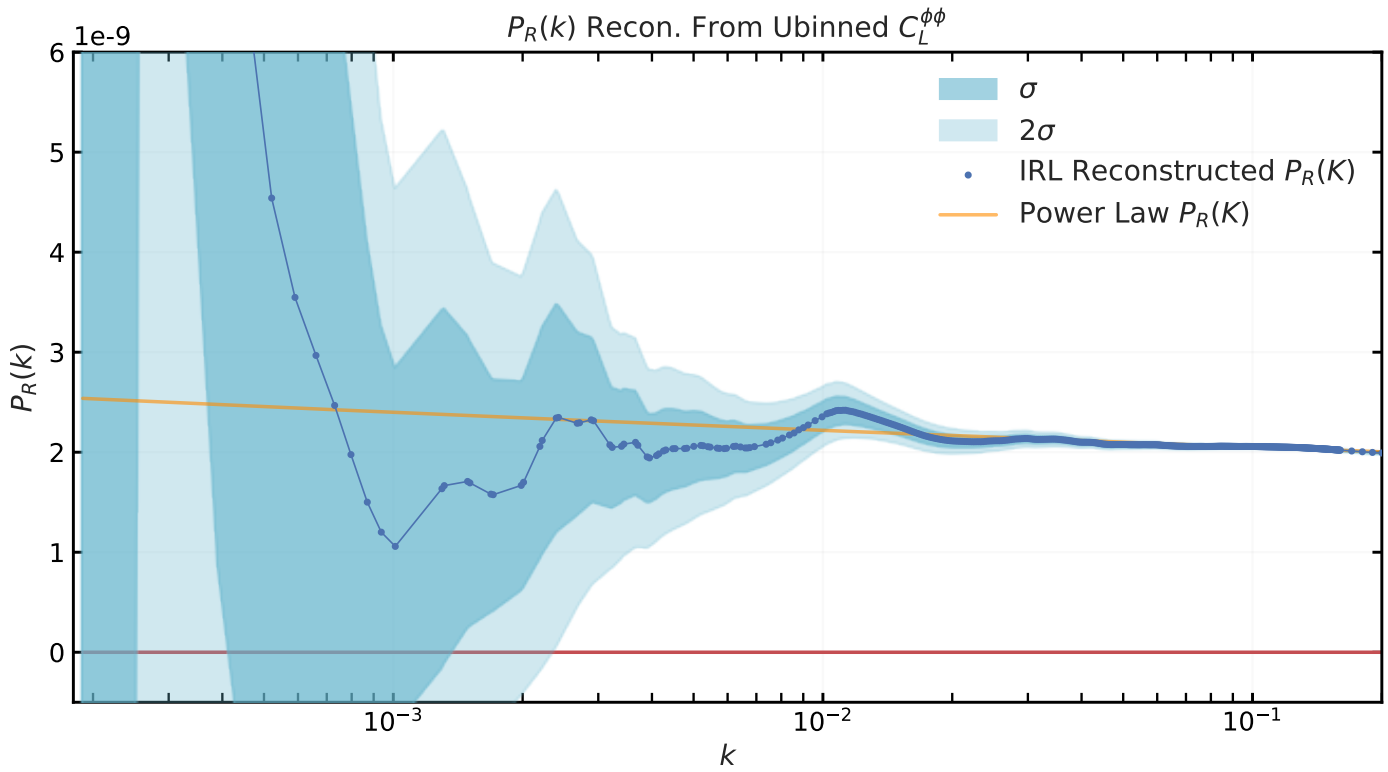

Figure: Plot of the reconstructed $P_R(k)$ (Blue) with $1\sigma, 2\sigma$ bands from 2×10^6 data realisations with cosmic variance error, overplotted on the fiducial Power Law $P_R(k)$ (Orange).[4]

Sparse $P_R(k)$ Reconstructed $C_L^{\kappa\kappa}$

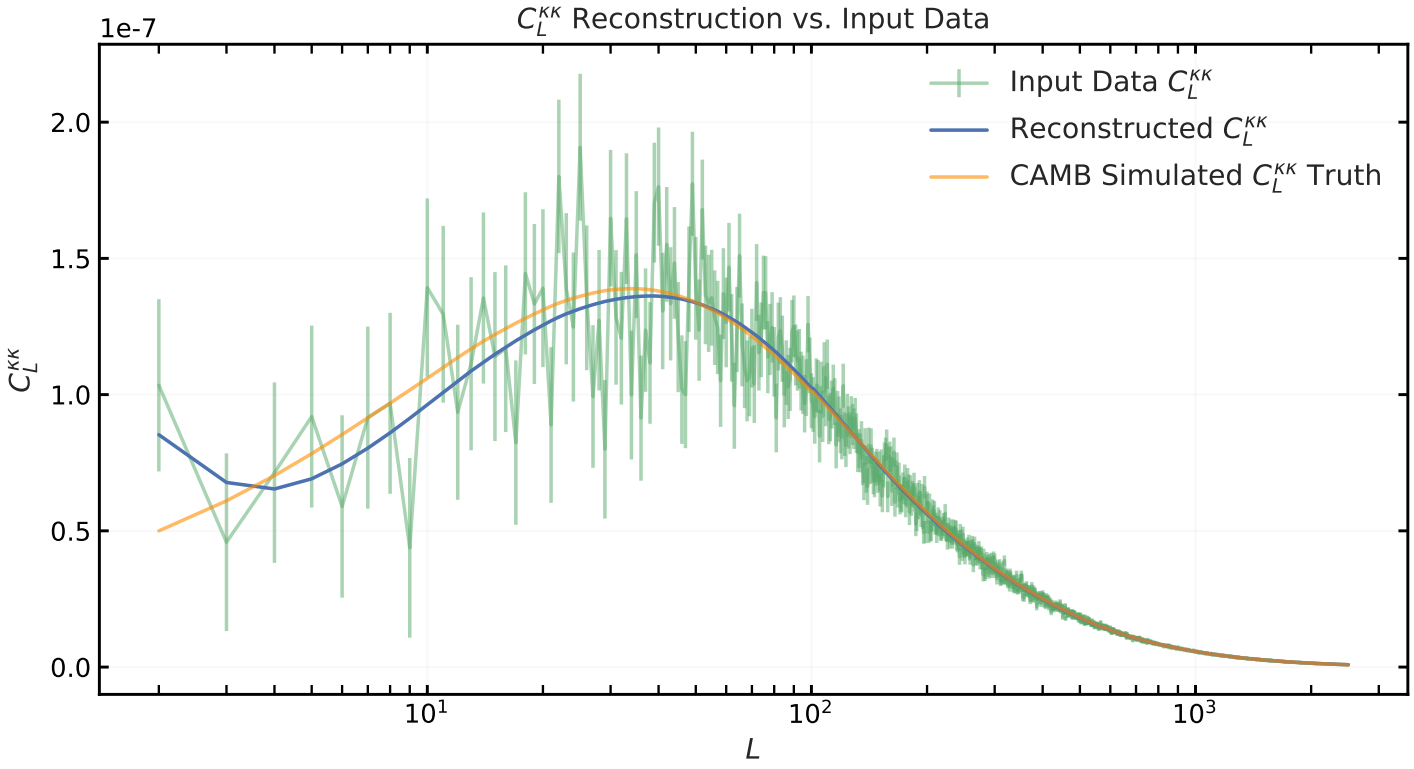

Figure: Reconstructed $C_L^{\kappa\kappa}$ in Blue plotted over the fiducial CAMB $C_L^{\kappa\kappa}$ in Orange and the input data realisation in Green.

Sparse $P_R(k)$ and $C_L^{\kappa\kappa}$ Reconstruction Error

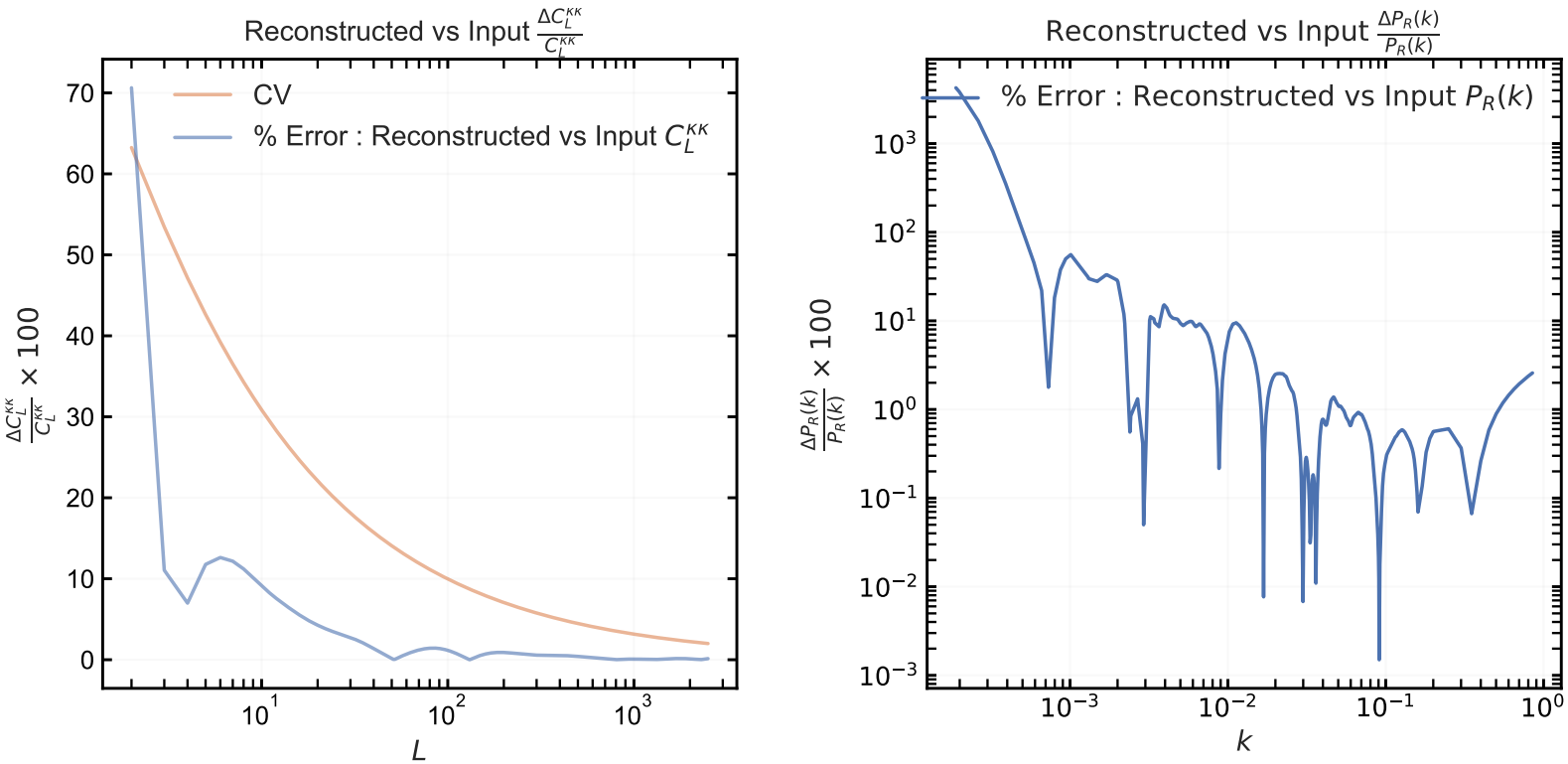

Figure: The two figures show the relative % error between the reconstructed $C_L^{\kappa\kappa}$ vs data realisation $C_L^{\kappa\kappa}$, and the reconstructed $P_R(k)$ vs input Power Law $P_R(k)$

Sparsely Reconstructed $P_R(k)$ Covariance Matrix

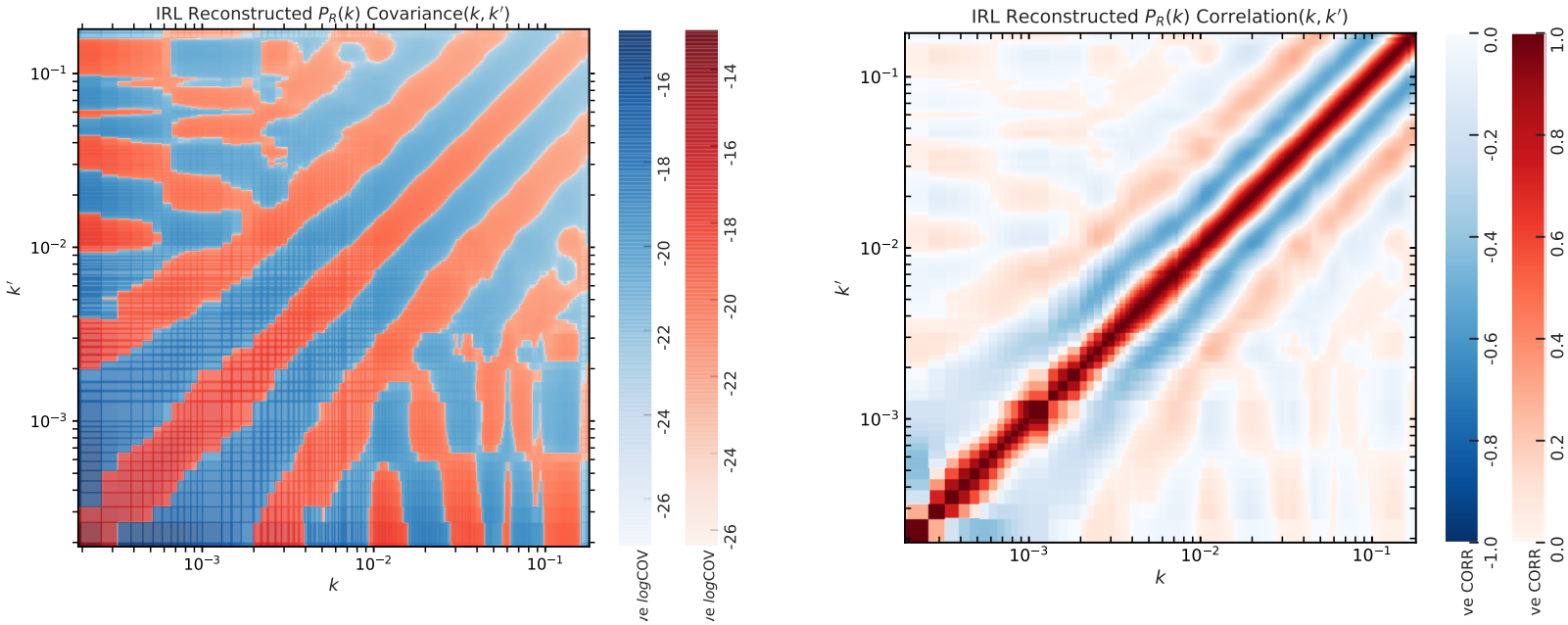

(a) **(b)**

Figure: a) is a plot of the $\Sigma_{kk'}$ from the reconstructed $P_R(k)$. Reds and Blues denote $\pm \log_{10} \Sigma_{kk'}$ respectively. Plot b) plots the correlations matrix $\rho_{kk'}$ with the Reds, Blues being the $\pm 0 \to 1$ range respectively.

Sparse $P_R(k)$ Covariance Singularity Test

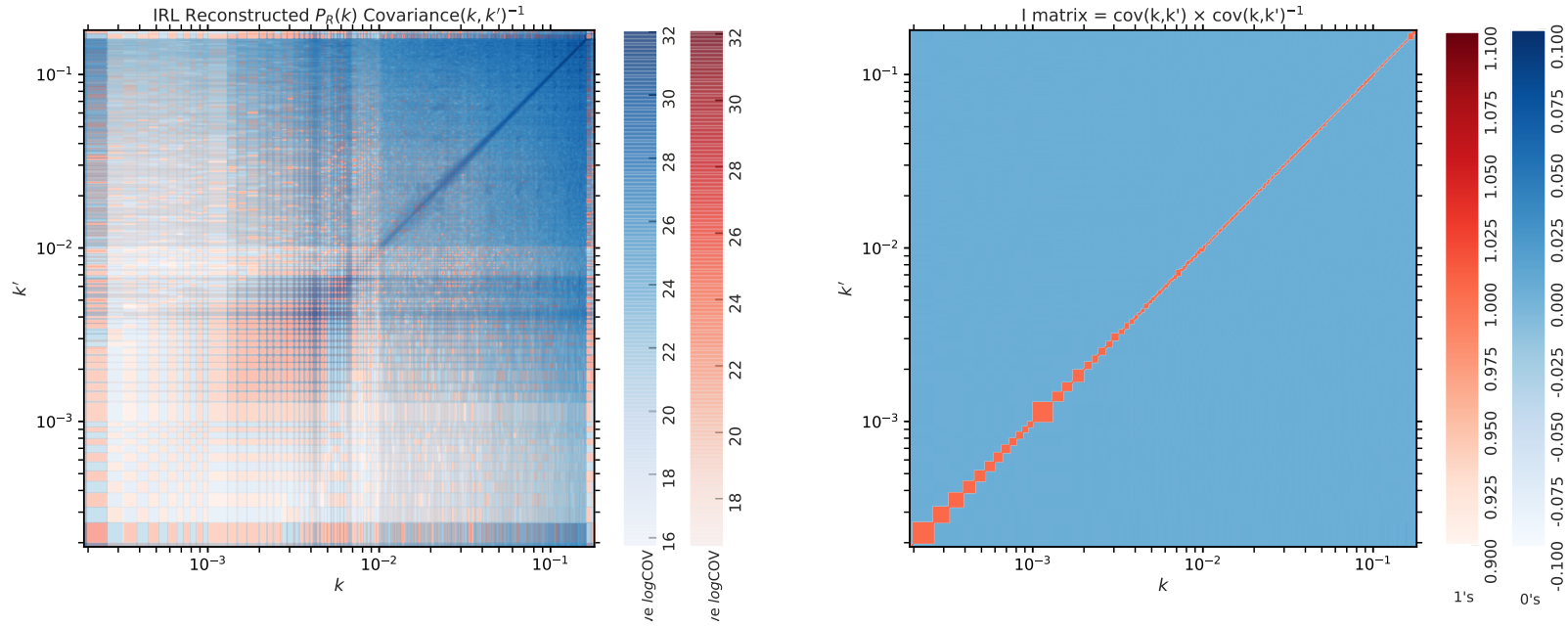

(a) **(b)**

Figure: a) Plots the $\Sigma^{-1}_{kk'}$. b) plots the $\Sigma_{kk'} \times \Sigma^{-1}_{kk'}$ with Reds, Blues being 1 ± 0.1, 0 ± 0.1 respectively. A clear Identity matrix is obtained within numerical bounds, showing that the $\Sigma_{kk'}$ is obtained from a unique $P_R(k)$ solution.

Conclusion

- $C_L^{\kappa\kappa}$ data from the latest surveys provides a new window into the reconstruction of $P_R(k)$
- The Richardson-Lucy estimator is a powerful model independent algorithm to carry out said reconstruction
- Sparsity algorithms based on the convolution kernel information can be used to optimize reconstruction and provide meaningful statistical verification
- $C_L^{\kappa\kappa}$ can potentially be used to cross reference reconstructions of $P_R(k)$ from other data sectors and verify points of interests such as low L power suppression in C_L^{TT}
- Cosmic Variance limited simulations give the best unbinned statistical budgets, with an expected reconstruction of medium to poor precision at low k to extremely high precision at high k.
- This $P_R(k)$ reconstruction sector appears to be of interest for future full sky missions where lensing reconstruction is a key feature.

N. Aghanim et al. “Planck 2015 results. XI. CMB power spectra, likelihoods, and robustness of parameters”. In: *Astron. Astrophys.* 594 (2016), A11. DOI: 10.1051/0004-6361/201526926. arXiv: 1507.02704 [astro-ph.CO].

Antony Lewis and Anthony Challinor. “Weak gravitational lensing of the cmb”. In: *Phys. Rept.* 429 (2006), pp. 1–65. DOI: 10.1016/j.physrep.2006.03.002. arXiv: astro-ph/0601594 [astro-ph].

Dhiraj Kumar Hazra, Arman Shafieloo, and Tarun Souradeep. “Primordial power spectrum from Planck”. In: *JCAP* 11 (2014), p. 011. DOI: 10.1088/1475-7516/2014/11/011. arXiv: 1406.4827 [astro-ph.CO].

Rajorshi Sushovan Chandra and Tarun Souradeep. “Primordial Power Spectrum Reconstruction From CMB Weak Lensing Power Spectrum”. In: (Apr. 2021). arXiv: 2104.12253 [astro-ph.CO].

D. Hanson et al. “CMB temperature lensing power reconstruction”. In: Phys. Rev. D 83.4, 043005 (Feb. 2011), p. 043005. DOI: 10.1103/PhysRevD.83.043005. arXiv: 1008.4403 [astro-ph.CO].